Nucleic Acids Research, 2023, **51**, 11104–11122
https://doi.org/10.1093/nar/gkad823
Advance access publication date: 19 October 2023
Genome integrity, repair and replication

ATM, KAP1 and the Epstein–Barr virus polymerase processivity factor direct traffic at the intersection of transcription and replication

Huanzhou Xu[1], Ibukun A. Akinyemi[2], John Haley[3], Michael T. McIntosh[2,4] and Sumita Bhaduri-McIntosh[1,4,*]

[1]Division of Infectious Diseases, Department of Pediatrics, University of Florida, Gainesville, FL 32610, USA
[2]Child Health Research Institute, Department of Pediatrics, University of Florida, Gainesville, FL 32610, USA
[3]Department of Pathology and Stony Brook Proteomics Center, Stony Brook University, Stony Brook, NY 11794, USA
[4]Department of Molecular Genetics and Microbiology, University of Florida, Gainesville, FL 32610, USA
[*]To whom correspondence should be addressed. Tel: +1 352 294 8879; Email: sbhadurimcintosh@ufl.edu

Abstract

The timing of transcription and replication must be carefully regulated for heavily-transcribed genomes of double-stranded DNA viruses: transcription of immediate early/early genes must decline as replication ramps up from the same genome—ensuring efficient and timely replication of viral genomes followed by their packaging by structural proteins. To understand how the prototypic DNA virus Epstein–Barr virus tackles the logistical challenge of switching from transcription to DNA replication, we examined the proteome at viral replication forks. Specifically, to transition from transcription, the viral DNA polymerase-processivity factor EA-D is SUMOylated by the epigenetic regulator and E3 SUMO-ligase KAP1/TRIM28. KAP1's SUMO2-ligase function is triggered by phosphorylation via the PI3K-related kinase ATM and the RNA polymerase II-associated helicase RECQ5 at the transcription machinery. SUMO2-EA-D then recruits the histone loader CAF1 and the methyltransferase SETDB1 to silence the parental genome via H3K9 methylation, prioritizing replication. Thus, a key viral protein and host DNA repair, epigenetic and transcription-replication interference pathways orchestrate the handover from transcription-to-replication, a fundamental feature of DNA viruses.

Graphical abstract

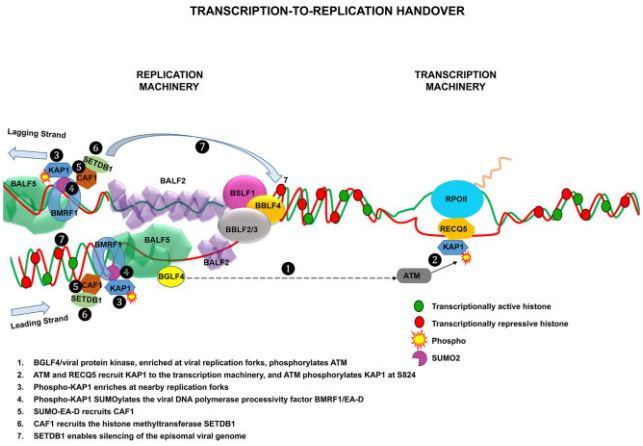

Introduction

DNA genomes are used as templates for both transcription and replication, presenting a potential for physical conflict between their respective machineries. Interference between DNA and RNA polymerases can result in DNA breaks and deleterious rearrangements, leading to disease. To avoid such consequences, cells have evolved mechanisms to temporally regulate transcription and replication. Such temporal regulation is equally important for DNA viruses that typically transcribe and replicate their genomes within a short window of time to ensure the production of infectious virus. In this regard, herpesviruses are the archetype. They remain latent or quiescent in their host but frequently emerge from latency via a process called reactivation to replicate their genomes and produce infectious virus particles (1). This lytic phase, that results from reactivation, is a highly regulated process that is characterized

Received: July 6, 2023. **Revised:** September 9, 2023. **Editorial Decision:** September 12, 2023. **Accepted:** September 20, 2023

by transcription of immediate early and early lytic genes from parental/episomal genomes followed closely by replication of those genomes using proteins encoded by early lytic genes. Newly replicated linear daughter genomes are then packaged using structural proteins that are transcribed largely from the new genomes. Promoter requirements and lack of heterochromatin ensure that late/structural genes are transcribed from newly replicated genomes, maintaining a temporal order (2). However, what regulates the transition from transcription of early genes to replication of the same genomic template is poorly understood.

The γ-herpesvirus Epstein–Barr virus (EBV) contributes to B, T and NK cell lymphomas as well as gastric and nasopharyngeal cell carcinomas, resulting in an overall ∼2% burden of human cancers (3). This cancer-causing virus is also an increasingly recognized trigger for multiple sclerosis (4). EBV, which infects nearly all humans, exhibits a biphasic life cycle in which it typically remains quiescent in B lymphocytes and like other herpesviruses, reactivates periodically from its latent state to produce a burst of viruses for dissemination. Reactivation is set off by a multitude of disparate triggers such as chemicals, hypoxia, IgG crosslinking, plasma cell differentiation and high glucose all of which culminate in transcription of the immediate early lytic switch gene *BZLF1* from the episomal viral genome (5,6). ZEBRA, the product of the *BZLF1* gene, is a replication protein and a transcription factor that transactivates many early lytic genes also from the episomal viral genome (7). Products of at least seven early lytic genes form the core virus replication machinery; these include the replication and transcription activator ZEBRA or Zta, the DNA polymerase (encoded by *BALF5*), the DNA polymerase processivity factor Early Antigen-Diffuse or EA-D (encoded by *BMRF1*), the single strand DNA binding protein (encoded by *BALF2*), the helicase (encoded by *BBLF4*), the primase (encoded by *BSLF1*) and the helicase-primase linker protein (encoded by *BBLF2/3*) (8,9). Transcription of these genes is therefore a prerequisite and must temporally precede replication of the episome. Importantly also, transcription of immediate early and early genes peaks before the bulk of herpesvirus genome replication occurs; therefore, immediate early and early gene transcription is turned down as genome replication ramps up (10–12). We hypothesized that clues to mechanisms that orchestrate this transcription-replication transition reside in the viral replication machinery itself, prompting us to examine replisomes on nascent viral DNA during the lytic phase.

Here, we report on the composition of the EBV replisome as the episomal genome reactivates from latency. We find that the EBV replisome is comprised of known viral replication proteins described above but also other viral proteins not expected at lytic forks. Two of these latter proteins are enzymes that cause a shift from the NTP to the dNTP pool. Additionally, cellular proteins contributing to DNA metabolism enrich at active forks while consistent with mainly late gene transcription, not replication, we find proteins important predominantly in RNA metabolism enriched on newly replicated genomes. Comparison to the replisome of the related but non-cancer-causing herpesvirus Herpes simplex virus 1 (HSV-1) highlights factors important in chromatin remodeling and in particular, KAP1, a prominent epigenetic silencer. Using KAP1 as a bait to address our original question, we discover that EBV functionally coordinates transcription and replication via its DNA polymerase processivity factor EA-D and four cellular enzymes ATM, RECQ5, KAP1 and SETDB1 to suppress transcription from episomal genomes, thereby mitigating transcription-replication interference and transitioning to genome replication.

Materials and methods

Cell lines

The EBV-postive Burkitt lymphoma (BL) cell line HH514-16 was a kind gift from Dr. George Miller at Yale University. EBV-transformed cell lines (LCL) were generated from healthy subjects as previously described (13,14). Both LCL and BL cell lines were maintained in RPMI 1640 (11875119, Gibco) supplemented with 10% fetal bovine serum (900108, GeminiBio) and 1% penicillin-streptomycin (15070063, Gibco). HEK293T-p2089 cells (293-EBV, human embryonic kidney cells bearing a wild-type EBV p2089 bacmid) were maintained with Dulbecco's modified Eagle medium (DMEM) (11965118, Gibco) supplemented with 10% fetal bovine serum and 1% penicillin-streptomycin. *BMRF1* knockout 293-EBV (B072-1) cell line (the *BMRF1* gene of the B95.8 EBV genome was deleted) was a kind gift from Professor Henri-Jacques Delecluse from the German Cancer Research Centre, Heidelberg, Germany. B072-1 cell line was maintained in RPMI 1640 supplemented with 10% fetal bovine serum, 1% penicillin-streptomycin and 50 μg/ml of hygromycin B (10687010, Invitrogen). All cell lines were incubated at 37°C in the presence of 5% CO_2.

Proliferation assay

BL cells were subcultured at 5×10^5 cells/ml and 24 h later, were treated with 3 mM sodium butyrate (NaB, 303430, Sigma Aldrich) for indicated durations. Cell numbers were counted by using trypan blue staining. Cell numbers were counted three times per condition.

Chemical treatment of cell lines

To induce lytic reactivation of EBV in BL cell line and LCL, cells were subcultured at 5×10^5 cells/ml, exposed to 3 mM NaB 24 h later, and harvested at indicated times. For experiments with α-amanitin (A2263, Sigma Aldrich), 5 μg/ml α-amanitin was added 18 or 24 h after NaB, and harvested after another 6 h. For experiments with KU-55933 (inhibitor of ataxia telangiectasia mutated, ATM), 3 mM NaB and 1 μM KU55933 (SML1109, Sigma Aldrich) were added 24 h after subculture, and harvested at indicated times.

Isolation of proteins on nascent DNA (iPOND)

1×10^8 HH514-16 cells were induced with NaB with or without 200 μg/ml of PAA for 36 h. Cells were pulse labeled with 10 μM EdU for 15 min. For chase, EdU labeled cells were washed once with 10 μM thymidine (Thy/Thymidine) containing medium and then incubated with 10 μM thymidine for 30 min prior to performing iPOND as described previously (15). Briefly, cells were harvested, washed once with PBS, fixed with 1% formaldehyde for 20 min at room temperature (RT), quenched with 0.125 M glycine for 5 min, permeabilized in 0.25% Triton X-100 in PBS for 30 min at RT, washed once with 0.5% BSA in PBS and once with PBS prior to performing click chemistry. For click chemistry, cells were incubated in 5 ml click reaction buffer (10 μM biotin-azide,

10 mM sodium ascorbate, 2 mM CuSO4) for 2 h at RT. DMSO was used instead of biotin-azide in negative control (no click [NC]) groups. Cells were centrifuged (900g, 5 min), washed once with 0.5% BSA in PBS and once with PBS. Nuclei were incubated in 1 ml of nuclear extraction buffer A (7006, Cell Signaling) in the presence of 0.5 μl 1M DTT and 1× protease inhibitor cocktail (7012, Cell Signaling) on ice for 15min. Samples were centrifuged (2000g, 5 min) at 4°C, washed once in 1 ml of buffer B (7007, Cell Signaling) containing 0.5 μl 1M DTT and re-suspended in 200 μl buffer B. To this, 1 μl of micrococcal nuclease (10011, Cell Signaling) was added and incubated for 20 min at 37°C with frequent mixing, followed by 10 μl of 0.5 M EDTA to stop the reaction. After centrifugation, nuclei were resuspended in cold lysis buffer (1% SDS, 50 mM Tris, pH 8.0), sonicated using a microtip sonicator at 8 W with 10-s on and 20-s off pulses on ice three times to break nuclear membranes. Samples were centrifuged at 16,000 × g for 10 min at 4°C to remove debris and diluted with the same volume of ice-cold PBS containing protease inhibitor cocktail (5871, Cell Signaling), and incubated with pre-washed 150 μl of streptavidin agarose beads (69203, EMD Millipore) overnight at 4°C. Protein-DNA complexes were either analyzed by mass spectrometry or eluted with 2 × Laemli buffer and boiled at 95°C for 25 min prior to performing immunoblotting.

For iPOND with 293T-EBV cells, cells in T75 flasks were transfected with 3 μg FLAG tagged EBV ORFs together with 3 μg each of HA-BZLF1 and HA-BRLF1 to induce EBV lytic reactivation for 36 h. Cells were pulse labeled with 10 μM EdU for 15 min with or without 10 μM thymidine for 30 min prior to performing iPOND and immunoblotting.

Liquid chromatography with tandem mass spectrometry (LC–MS/MS)

Protein-DNA complexes on beads were washed twice with ice cold TBS, transferred to a fresh polypropylene tube and washed once with TBS and once with cold water. Capture beads were resuspended in 100 μl 100mM ammonium bicarbonate pH 8 with 5mM DTT and heated to 90°C for 20 min. Cysteines were alkylated by addition of 10 mM iodoacetamide, incubated at RT for 30 min, and proteins digested with trypsin overnight at 37°C. Peptides were desalted on reverse phase spin tips (10 μl bed volume), dried, resuspended in 0.1% formic acid/water and subjected to LC–MS/MS.

Parent peptide mass, collision-induced fragment mass information and peptide abundance values were obtained by a liquid chromatography-electrospray ionization tandem mass spectrometry (LC–MS/MS) using an orbital trap instrument (Thermo Q-Exactive HF) followed by protein database searching. HPLC C18 columns were prepared using *P*-2000 laser puller (Sutter Instruments) and silica tubing (100 μm ID × ∼20 cm) and were self-packed with 3 μm Reprosil C 18 resin. Peptides were separated on the resolving column with a flow rate of 300 nL/min, using a gradient elution step 0−40% with acetonitrile (MeCN) and 0.1% formic acid (0.23%/min) over 40 min, followed by a 10 min wash with 90% MeCN and a 10 min wash step with isocratic 90% MeCN. Electrospray ionization was achieved using a spray voltage of 2.3 kV. Data-dependent MS and MS–MS acquisitions were made using a survey scan (m/z 375−1400) with maximum fill of 50 ms followed typically by 20 consecutive product ion scans (m/z 100−1600). Parent ion with charge states of 2+, 3+ and 4 + were selected with a 15 s exclusion period. MS data were collected using Xcaliber (Thermo).

Raw data were analyzed using Proteome Discoverer v2.2 software (Thermo) using label free quantitation. Resolution of MS and MS/MS data searches were set to 10 ppm and 0.05 Da respectively. Two skipped trypsin cleavages and M-oxidation, KR-deamidation, ST-dehydration modifications were allowed. Protein identifications were binned at <1% and <5% FDR cutoffs. A human + EBV UniProt dataset (74947 entries) was used for data alignment. Fold change ratios were obtained by matched peptide-based label free quantitation and *P*-values were calculated by Benjamini-Hochberg correction for FDR.

Identification of high confidence protein interactors of nascent DNA

Proteins with peptide spectra in fewer than three out of six experimental replicates from the yes click (YC) condition were excluded, and *P*-values were calculated by Student's *t* test applied to the average spectral abundances for each protein in YC compared to no click (NC) conditions (duplicate runs of six experimental replicates for each condition). Raw spectral abundance values for host and viral proteins identified by iPOND-MS were then converted to normalized spectral abundance factors (NSAF) and expressed as %NSAF according to Paoletti *et al.* (16). Average %NSAF values for each condition, YC, thymidine chase-clicked (THY), NC and PAA (PAA) treated were calculated as were ratios of the averages for YC and THY conditions each compared to NC and PAA combined averages. High confidence interacting proteins of nascent DNA were then determined using a cut-off *P*-value <0.05 and enrichment in YC or THY iPOND with $\log_2$FC >0.5 over background (NC and PAA conditions). Division by zero was corrected by substitution of 0 with 0.0001 for average NSAF values from some NC and PAA samples. Lists of high confidence proteins enriched in YC and THY chase samples were then compared in BioVenn (17) to reveal active replication fork proteins in (YC and THY enriched) versus new viral DNA associated proteins (THY enriched only).

Network analysis

Statistically significant biological processes were determined by overrepresentation analysis (ORA) and plotted according to the Enrichment ratio score for each gene set and biological process using WebGestalt 2019 (18). Statistically significant EBV iPOND cellular proteins were also subjected to STRING analysis (19) to identify high confidence interactions.

Cross-species comparison between EBV and HSV interactors

A cross platform analysis comparing putative functional and physical interactomes of twenty-one cellular proteins in common at EBV replication forks and the previously published nascent HSV-1 genome in an infection model (20) was also completed using BioVenn followed by STRING analysis.

Plasmids, siRNA and transfection

The plasmids used in this study are listed in the key resource table. HA-BZLF1 and HA-BRLF1 were constructed by subcloning *BZLF1* and *BRLF1* into vector pcDNA3.1-StrepHA. Mutants of FLAG-BMRF1 (K135R and K212R) were

constructed by overlapping extension PCR. The primers used for constructing HA-BZLF1 and HA-BRLF1 are as following: 5′CAGCGGATATCATGATGGACCCAAACTCGAC3′ (forward) and 5′ACTCGAGCGGCCGCTTAGAAAT TTAAGAGATCCTCGTGT3′ (reverse) for HA-BZLF1; 5′CAGCGGATATCATGAGGCCTAAAAAGGATGGC3′ (forward) and 5′ACTCGAGCGGCCGCCTAAAATAAGCT GGTGTCAAAAATAG3′ (reverse) for HA-BRLF1.

For transfection of BL cell line, cells were subcultured at 5×10^5 cells/ml for 24 h. Cells were washed once with PBS and nucleofected with 200 pmol siRNA using an Amaxa Nucleofector II (program A-024) as described previously (21). The siRNAs used in this study are listed in the Key Resources table.

For 293-EBV and B072-1 cell lines, cells were seeded in T75 flasks 24 h before transfection at which time 3 μg of FLAG-BZLF1 or HA-BZLF1 and 3 μg of FLAG-BRLF1 or HA-BRLF1 were transfected to induce EBV lytic reactivation by using LipoJet™ In Vitro Transfection Kit (SL100468) according to manufacturer's instructions.

Immunoblotting

Immunoblotting was performed as described previously (22). Briefly, cells were lysed in RIPA buffer with protease inhibitors. Cell lysates were electrophoresed on SDS-polyacrylamide gels, transferred to nitrocellulose membranes and probed with indicated antibodies. Antibodies used in this study are listed in the Key Resources table.

Quantitative reverse transcriptase-PCR (RT-qPCR)

RT-qPCR was performed as described previously (23). Briefly, 1 μg of total RNA was used as template to synthesize complementary DNA using MuLV reverse transcriptase (M0253L, New England Biolabs). Quantitative PCR was used to assay relative transcript levels using the following primers: 5′GTAACCCGTTGAACCCCATT3′ (forward) and 5′CCATCCAATCGGTAGTAGCG3′ (reverse) for 18S rRNA; 5′TTCCACAGCCTGCACCAGTG3′ (forward) and 5′GGCAGAAGCCACCTCACGGT3′ (reverse) for *BZLF1*; 5′ACCTGCCGTTGGATCTTAGTG3′ (forward) and 5′GGCGTTGTTGGAGTCCTGTG3′ (reverse) for *BMRF1*. Data were analyzed by normalizing to 18S rRNA using the ΔΔCT method.

Quantitative PCR (qPCR) to analyze EBV genomic DNA

EBV genomic DNA was measured using qPCR to amplify *BALF5* as described previously (21). To distinguish newly synthesized EBV genomes from parental episomal genomes, viral genomic DNA was extracted from BL cells 24 h after transfection using the DNeasy kit (K182001, Invitrogen). DNA was treated with MboI at 37°C overnight to digest newly replicated unmethylated DNA prior to amplifying the *BALF5* gene by qPCR using the following primers that spanned an MboI site: 5′GCCATCCAAAGCATTCGCAT3′ (forward) and 5′GATTACGCCAAGCGCGCAA3′ (reverse). For EBV lytic replication assays, 1 μg each of FLAG-BZLF1 and FLAG-BRLF1 together with 1 μg of FLAG-BMRF1 (WT) or mutants (K135R, K212R) were transfected into B072-1 cells using the LipoJet transfection kit (SL100468, SignaGen) according to manufacturer's protocol. Total genomic DNA was extracted and viral DNA was measured by amplifying the EBV *BALF5* gene with the following primers: 5′CGTCTCATTCCCAAGTGTTTC3′ (forward) and 5′GCCCTTTCCATCCTCGTC3′ (reverse).

Immunoprecipitation analysis

Immunoprecipitation was performed as described previously (21). In brief, cells were lysed in immunoprecipitation Lysis Buffer (87787, Thermo Scientific) with protease inhibitors for 10 min on ice and spun down at 4°C for 5 min. After removing the supernatant to new eppendorf tubes, 5% of the material was set aside as input; the rest was incubated with indicated antibodies (or the same amount of control IgG) and 30 μl of Dynabeads Protein G (10003D, Thermo Scientific) at 4°C overnight. Beads were washed three times with immunoprecipitation lysis buffer prior to immunoblotting.

SUMOylation co-immunoprecipitation analysis

SUMOylation assay was performed as described previously (24). Briefly, cells were lysed with immunoprecipitation lysis buffer with protease inhibitors and 20 mM *N*-ethylmaleimide (NEM) on ice for 10 min and spun down at 4°C for 5 min. The supernatant was then processed as in the Immunoprecipitation analysis above except that anti-SUMO antibodies (listed in the Key Resources table) were used to enrich SUMOylated proteins followed by immunoblotting.

Chromatin immunoprecipitation-quantitative PCR (ChIP-qPCR)

ChIP was performed as described previously (25). A total of 4×10^6 cells were treated with NaB (with or without depletion of RECQ5) for 24 h prior to performing ChIP in Figure 7A–D. Cells were treated with NaB for 24 h followed by exposure to α-amanitin for 6 h prior to performing ChIP in Figure 4D. DNA was purified using spin columns (14209S, Cell signaling) according to the manufacturer's protocol. Eluted DNA was cleaved with MboI (R0147S, New England Biolabs) to remove newly synthesized EBV genomes prior to performing qPCR. The antibodies and primers used for ChIP-qPCR are listed in the Key Resources table.

Cell cycle analysis by flow cytometry

HH514-16 cells were induced with or without NaB for indicated times and subjected to flow cytometry. For intracellular staining, cells were fixed with Cytofix/Cytoperm solution (554722, BD Biosciences) for 15 min on ice and washed twice with perm/wash buffer (554723, BD Biosciences). Cells were then stained with indicated primary and secondary antibodies. After two washes with the perm/wash buffer, cells were re-suspended in PBS and subjected to flow cytometric analysis.

For cell cycle analysis, described previously (15), cells were incubated with 100 μM BrdU 1 h prior to harvest and spun down. After fixation with 70% ethanol in PBS at –20°C for 1 h and denaturation with 2 N HCl/0.5% Triton X-100 at room temperature for 30 min, cells were stained with an anti-BrdU antibody followed by FITC-conjugated anti-mouse antibody. Cells were resuspended in PBS containing 10 μg/ml RNase A (EN0531, Thermo Scientific) and 20 μg/ml propidium iodide (PI, P4864, Sigma) for 1 h at room temperature in the dark prior to analyzing by flow cytometry. Antibodies are listed in the Key Resources table.

KEY RESOURCES TABLE

REAGENT or RESOURCE	SOURCE	IDENTIFIER
Antibodies		
Anti-EBV EA-D-p52/50 Antibody, clone R3	Miilipore-Sigma	MAB8186
Mouse anti-β-actin antibody (AC-15)	Sigma-Aldrich	A1978
Mouse anti-ZEBRA antibody (BZ1)	a gift from Professor Paul Farrell	NA
Rabbit anti-ZC3H18 antibody	Bethyl Laboratories	A304-682A
Rabbit anti-KAP1 antibody	Bethyl Laboratories	A300-274A
Rabbit anti-phospho KAP-1 (S824) antibody	Bethyl Laboratories	A300-767A
Rabbit anti-SUMO2 antibody	Novus Biologicals	NBP1-77163
Rabbit anti-SUMO1 antibody	Cell Signaling Technology	4930
Mouse anti-FLAG antibody	Sigma-Aldrich	F1804
Mouse anti-HA antibody	Sigma-Aldrich	H3663
Rabbit anti-RECQ5 antibody	Bethyl Laboratories	A302-520A
Rabbit anti-PCNA antibody	Bethyl Laboratories	A300-277A
Rabbit anti-phospho-Histone H2AX (Ser139) antibody	Cell Signaling Technology	9718S
Rabbit anti-ATM antibody	Bethyl Laboratories	A300-299A
Rabbit anti-RNA polymerase II antibody	Cell Signaling Technology	14958S
Rabbit anti-Caf1p150 antibody	Bethyl Laboratories	A301-482A
Rabbit anti-EHMT2 antibody	Proteintech	29303–1-AP
Rabbit anti-SUV39H2 antibody	Proteintech	11338–1-AP
Rabbit anti-EHMT1 Antibody	Bethyl Laboratories	A301-642A-T
Rabbit anti-SUV39H1 antibody	Proteintech	10574–1-AP
Rabbit anti-SETDB1 antibody	Proteintech	11231–1-AP
rabbit anti-Tri-Methyl-Histone H3 (Lys9) (H3K9me3) antibody	Cell Signaling Technology	13969S
rabbit anti-Tri-Methyl-Histone H3 (Lys27) (H3K27me3) antibody	Cell Signaling Technology	9933T
Rabbit anti-Tri-Methyl-Histone H3 (Lys4) (H3K4me3) antibody	Cell Signaling Technology	9751S
Rabbit anti-Acetyl-Histone H3 (Lys9) (H3K9Acetyl) antibody	Cell Signaling Technology	9649S
Rabbit anti-Histone H3.1 antibody	Novus Biologicals	NBP2-75524
Mouse anti-BrdU antibody	BD Biosciences	555627
Mouse IgG1	BD Biosciences	557273
Rabbit IgG	R&D	AB-105-C
FITC-conjugated goat anti-mouse IgG	Sigma-Aldrich	F0257
FITC-conjugated goat anti-rabbit IgG	Sigma-Aldrich	F0382
Human IgG APC-conjugated antibody	R&D	F0135
HRP-conjugated goat anti-mouse IgG(H + L)	Thermo Fisher Scientific	626520
HRP-conjugated goat anti-rabbit IgG(H + L)	Thermo Fisher Scientific	31460
Major commercial kits		
QiAquick PCR Purification Kit	Qiagen	28106
QIAquick Gel Extraction Kit	Qiagen	28704
Box of Engraved Combicoverslips (x50) RUO	Genomic Vision	COV-002-RUO
FiberPrep® (DNA Extraction Kit)	Genomic Vision	EXT-001
QIAprep Spin Miniprep Kit	Qiagen	27106
PureLink™ Genomic DNA Mini Kit	Invitrogen	K182001
RNeasy RNA extraction kit	Qiagen	74104
Plasmid Maxi Kit	Qiagen	12262
Power SYBR Green PCR Master Mix	Life Technologies Corporation	A25778
Mirus Bio™ Ingenio™ Electroporation Solution	Fisher scientific	MIR50117
LipoJet™ In Vitro Transfection Kit	SignaGene Laboratories	SL100468
Chemicals		
Sodium butyrate	Sigma Aldrich	303430
Hygromycin B	Sigma Aldrich	10687010
α-amanitin	Sigma Aldrich	A2263

KEY RESOURCES TABLE

REAGENT or RESOURCE	SOURCE	IDENTIFIER
KU-55933	Sigma Aldrich	SML1109
N-Ethylmaleimide (NEM)	Sigma-Aldrich	E3876
Recombinant DNA		
FLAG-KAP1	a kind gift from Professor Kum Kum Khanna	NA
FLAG-BZLF1	a kind gift from Dr Kathy Shair	NA
FLAG-BRLF1	a kind gift from Dr Kathy Shair	NA
FLAG-BKRF4	a kind gift from Dr Kathy Shair	NA
FLAG-BKRF3	a kind gift from Dr Kathy Shair	NA
FLAG-BNRF1	a kind gift from Dr Kathy Shair	NA
FLAG-BcLF1	a kind gift from Dr Kathy Shair	NA
FLAG-BLLF3	a kind gift from Dr Kathy Shair	NA
FLAG-BORF2	a kind gift from Dr Lori Frappier	NA
FLAG-BMRF1	a kind gift from Dr Kathy Shair	NA
FLAG-BGLF4	a kind gift from Dr Kathy Shair	NA
FLAG-BGLF5	a kind gift from Dr Kathy Shair	NA
FLAG-SENP1	a gift from Edward Yeh (Addgene plasmid # 17357; http://n2t.net/addgene:17357;RRID:Addgene_17357) (30)	17357
HA-SUMO2	a gift from Ying Liu (Addgene plasmid # 66867; http://n2t.net/addgene:66867;RRID:Addgene_66867) (31)	66867
HA-BZLF1	This study	NA
HA-BRLF1	This study	NA
FLAG-BMRF1 (K135R)	This study	NA
FLAG-BMRF1 (K212R)	This study	NA
siRNAs		
si*KAP1* #1	Santa Cruz	sc-38550
siKAP1 #2	Ambion	107830,
si*ATM*	Ambion	118231,
si*RECQ5* #1	Ambion	137517
siRECQ5 #2	Ambion	137518
si*SETDB1* #1	Ambion	S19111
si*SETDB1* #2	Ambion	S19112
scramble siRNA (siCtrl)	Dharmacon	D001810-01-20
si*PCNA*	Ambion	143722
Primers		
Gene name	Forward primers (5′∼3′)	Reverse primers (5′∼3′)
BZLF1 promoter	TTCAGCAAAGATAGCA AAGGT	ACTTCTGAAAACTGCC TCCT
BZLF1 gene body	GACCCATACCAGGTGC CTTTTG	GCACACAAGGCAAAGG AGCTTG
BRLF1 promoter	GGGCTGTTCCTGGCAA GAGT	GGGGGAGTAGTAGCTT AGCAGC
BRLF1 gene body	ACCGGTTCATGGACAG GTCC	TTCGAGGGGCGAGAGG TGTG
BMRF1 promoter	AGCATGACAGCCAAGG CTGA	ACCAAGGTAACCCCCT CTCC
BMRF1 gene body	GCATCATAGCTGTGGT GGCC	TCTGGCTCAGAGGCCG TACT
BALF5 promoter	ATTTCCCTCACGAGGC GCA	ATGGGATTAATGCCTG GACCCTCA

DNA fiber assay

DNA fiber assay was performed by using FiberPrep DNA Extraction Kit (EXT-001, Genomic vision) as described previously (26). Briefly, 293T-EBV cells were transfected with scrambled siRNA or si*KAP1* together with FLAG-BZLF1 and FLAG-BRLF1 to induce EBV lytic reactivation for 36 h. Cells were pulsed with 250 μM IdU (I7125, Sigma) for 30 min followed by trypsinization and two washes with PBS. 400,000 cells were resuspended in low-melting point agarose together with 0.5% trypsin and solidified in a plug mold at 4°C for 2 h. Plugs were then digested with proteinase K at 50°C overnight and washed four times with 0.01 M Tris–EDTA. DNA fibers were combed to coverslips (COV-002-RUO, Genomic Vision)

using the FiberComb Molecular Combing System. Fibers were baked at 60°C for 2 h and denatured in 0.5 M NaOH/1 M NaCl for 8 min prior to staining with mouse anti-BrdU antibody (347580, BD Biosciences) for 1h and goat anti-mouse Alexa Fluor 488 antibody (A11001, Thermo fisher scientific) for 45 min. Coverslips were dehydrated in 70%, 90% and then 100% ethanol for 1 min each prior to mounting on slides. DNA fiber images were acquired using a fluorescence microscope (OLYMPUS) equipped with a OLYMPUS U-TV 0.63XC digital camera and analyzed with ImageJ software (27).

Proximity ligation assay (PLA)

PLA was performed following a previously described protocol (28). Briefly, cells were induced with NaB with/without PAA (200μg/ml) for indicated times and fixed with Cytofix/Cytoperm solution for 15 min on ice. After two washes with perm/wash buffer, cells were incubated with indicated primary antibodies for 1 h at room temperature, washed twice again with perm/wash buffer, incubated with PLUS and MINUS PLA probes (DUO92006 and DUO92002, Sigma) for 1 h and washed with buffer A (DUO82049, Sigma). Cells were incubated with ligation mixture (DUO94002, Sigma), washed twice with buffer A and incubated with amplification reaction for 100 min followed by two washes with buffer B (DUO82049, Sigma). Cells were then incubated with mouse anti-ZEBRA antibody and Allophycocyanin (APC) conjugated goat anti-mouse antibody for 45 min. Cells were mounted to slides with DAPI prior to acquiring images using a fluorescence microscope (OLYMPUS) equipped with an OLYMPUS U-TV 0.63XC digital camera.

Bromouridine-RT-qPCR (BrU-RT-qPCR) for nascent transcript analysis

BrU-RT-qPCR was performed as previously described (29). Briefly, 5×10^6 BL cells were transfected with si*RECQ5* or scrambled siRNA for 20h and then induced with NaB for 24 h. Cells were incubated with 2 mM BrU (850187, Sigma) for 30 min before collecting. Total RNA was extracted using TRIzol (15596-018, Invitrogen) and incubated with 2 μg mouse anti-BrdU antibody (555627, BD Biosciences), 50 μl goat anti-mouse IgG magnetic Dynabeads (11033, Invitrogen) in 0.1% BSA/PBS and 20 U RNaseOUT (10777019, Invitrogen) for 1h. Beads were washed three times with 0.1% BSA/PBS, resuspended in 40 μl nuclease free water, and then heated at 80°C for 10 min to elute BrU-labeled RNA. Then, 1 μg BrU labeled RNA was used as template to synthesize cDNA followed by qPCR to amplify transcripts of *BZLF1 and BMRF1* using the following primers: 5′TTCCACAGCCTGCACCAGTG3′ (forward) and 5′GGCAGAAGCCACCTCACGGT3′ (reverse) for *BZLF1*; 5′ACCTGCCGTTGGATCTTAGTG3′ (forward) and 5′GGCGTTGTTGGAGTCCTGTG3′ (reverse) for *BMRF1*.

Statistical analysis

Student's *t* test was used to assess statistical significance when performing pair-wise comparisons. Results are expressed as the mean ± standard error of the mean (SEM) for at least triplicate experiments unless indicated otherwise. P values were calculated using Microsoft Excel or GraphPad Prism5; *P* value of <0.05 was regarded as statistically significant. For DNA fiber analysis, *P* values were calculated using two tailed Mann–Whitney *U* tests.

Results

Lytic reactivation from EBV latency halts host genome replication.

Extrachromosomal circular EBV genomes reside in the nucleus in a silent/latent state and are replicated alongside the host genome by the cellular DNA replication machinery (32). This ensures transfer of the latent viral genome to daughter B lymphocytes. However, to propagate itself, the viral genome switches to the productive/lytic phase in which the viral replication machinery, expressed from the viral genome early in the lytic phase, replicates the genome to produce large quantities of unchromatinized linear viral DNA (33). To isolate the replication machinery at viral forks during the lytic phase, we needed to confirm that consistent with previously published reports (34–41), cellular DNA replication was indeed blocked upon exposure to a lytic trigger known to robustly activate the viral lytic phase. We therefore exposed latently-infected Burkitt lymphoma (BL) cells to sodium butyrate (NaB), a potent trigger of the lytic switch, and observed that the lytic phase was activated as expected by expression of the latent-to-lytic switch protein ZEBRA and the early lytic protein EA-D in the absence or presence of phosphonoacetic acid (PAA) which blocks downstream viral DNA replication (Supplementary Figure S1A); PAA is a viral DNA polymerase inhibitor which is known not to impact expression of immediate early and early lytic genes (42). BrdU uptake experiments demonstrated a dearth of replicating cells among those refractory to lytic reactivation by NaB at 24 and 36 h (Supplementary Figure S1B; note robust replication of control uninduced cells); however, consistent with viral DNA replication commencing around 24 h and increasing significantly by 36 h (Supplementary Figure S2A, B; note the expected inhibition of viral DNA replication by PAA), increased BrdU uptake was observed from 24 to 36 h in lytic cells (Supplementary Figure S1B). Also supporting a lack of cellular DNA replication in both lytic and refractory cells, we observed very little cell proliferation after exposure to NaB (Supplementary Figure S1C), further confirming previous observations of cell cycle arrest prior to herpesvirus DNA replication during the lytic phase (34–41). We also confirmed that as previously described (10–12), and in contrast to an increase in viral DNA replication (Supplementary Figure S2A, B), the abundance of immediate early (*BZLF1*, *BRLF1*) and early (*BMRF1*) transcripts decreased significantly from 24 to 36 h (Supplementary Figure S2C); though, as expected, the abundance of *BFRF3*, a late transcript, rose alongside DNA replication from 24 to 36 h (Supplementary Figure S2C). Thus, consistent with prior understanding, transcription of immediate early and early genes from the episome is indeed turned down as replication ramps up.

EBV proteins at viral replication forks

The cell cycle arrest known to occur prior to viral DNA replication (34–41) and our results (in Supplementary Figure S1B, C) indicated that viral genomes, not cellular genomes, replicated in lytically reactivated cells. To purify such replicating EBV DNA from lytically reactivated BL cells and lymphoblastoid cell lines (LCL), we used isolation of proteins on nascent DNA (iPOND; Supplementary Figure S1D). Earlier studies on lytic processes predominantly used cell biology approaches to image replication complexes labeled via

in situ hybridization of viral DNA or antibodies targeting viral replication proteins. These complexes are sites of viral gene transcription, DNA synthesis, capsid assembly and other processes needed to complete the lytic cycle; as such, these methodologies preclude finer distinction between the precise contents and their functions during the lytic phase. We therefore used iPOND, a more granular and dynamic assay that focuses on DNA replication and distinguishes between actively replicating and newly replicated DNA (by chasing with an unlabeled nucleoside e.g. thymidine). We subjected iPOND-derived viral forks from lytically reactivated BL cells and LCL to immunoblotting; we used these two cell lines to increase rigor and because LCL carry type 1 EBV while these BL cells carry type 2 EBV. As expected, we found that the viral replication proteins EA-D, ZEBRA and viral DNA polymerase were enriched at replication forks; however, the host protein ZC3H18, previously identified at cellular forks of latently-infected BL cells and LCL (15), was not enriched at viral forks (Supplementary Figure S1E and 1F). Importantly also, the host DNA polymerase delta, a workhorse of cellular DNA replication that has essential functions on the lagging strand of the replication fork, was missing from these forks (Figure 1F). As expected also, when viral DNA replication was blocked using PAA, viral replication proteins were poorly enriched or absent (Supplementary Figure S1E-G), providing further support for specific enrichment of viral replication forks by iPOND following lytic reactivation. This was in contrast to our earlier study in which we did the opposite, i.e. enriched primarily cellular DNA replication forks but no viral DNA forks (15).

When iPOND samples were analyzed by mass spectrometry, several viral lytic proteins, expected at replication forks (Figure 1A), were identified (Figures 1B-E). These included replisome proteins and proteins previously found to participate in viral DNA replication such as the products of *BALF2*, *BALF5*, *BMRF1*, *BZLF1*/ZEBRA, *BRLF1* (replication and transcription activator, RTA), *BGLF4* (protein kinase) and *BGLF5* (nuclease) (8,43–45). Notably, while components of the cellular pre-replication complex (MCM2-7) were also identified, cellular DNA polymerases were not, indicating potentially abortive replication of viral genomes from the latent origin of replication and/or pointing to previously unknown functions of MCM proteins at lytic forks. Several viral capsid proteins and proteins important in viral packaging were also identified likely due to enrichment at newly replicated DNA. Figures 1F–H show select viral proteins that were validated at forks using iPOND-immunoblotting following introduction of FLAG-tagged EBV ORFs into EBV bacmid-bearing (293-EBV) cells that had been lytically activated by simultaneous introduction of HA-tagged *BZLF1* and *BRLF1*. Some of these proteins persisted on newly replicated (thymidine chased) genomes while others did not. Two proteins of interest were products of *BLLF3* and *BORF2*. *BLLF3* encodes a dUTPase that hydrolyzes dUTP to dUMP, thereby providing the substrate for thymine nucleotide synthesis. *BORF2* encodes the large subunit of the ribonucleotide reductase which converts nucleotides to deoxynucleotides needed for DNA synthesis (46,47). These experiments demonstrated occupancy of several EBV lytic proteins on replicating viral genomes and in particular, two viral proteins that are known to shift the nucleotide pool from NTP to dNTP precursors, thus favoring DNA replication.

Cellular proteins at viral replication forks

Mass spectrometry of iPOND samples (three to six replicates) from lytically reactivated cells revealed 231 cellular proteins at active forks (Table S1). Of the 229 cellular proteins identified following thymidine chase (Table S2), 61 were unique to chased samples i.e. enriched on newly replicated viral genomes (Figure 2A). Of note, newly replicated viral genomes are linear and serve as templates for transcription of late/structural gene products. Accordingly, while proteins contributing to DNA metabolism were largely enriched at active viral forks, contributors to RNA metabolism coenriched with newly replicated genomes (Figures 2B and C). These findings are consistent with robust virus genome replication ∼36 hours post reactivation (Supplementary Figure S2A, B), an event to which late gene transcription is temporally tied (48). Interactome analyses of fork-associated proteins revealed four functional/biological pathways corresponding to DNA replication & repair, chromatin modification & transcriptional repression, RNA processing and proteasome (Figure 2D). Cross-analysis of our data against a previously published proteome at nascent viral genomes from an HSV-1 infection model (20) highlighted two pathways: chromatin modification & transcriptional repression (eleven proteins) and DNA mismatch repair (seven proteins). Three additional proteins THOC2, PDS5B and TOP1 are involved in RNA processing, chromatin cohesin complex, or DNA unwinding, respectively (Figure 2E).

Given our objective of identifying mechanisms that silence immediate-early and early gene transcription to make way for DNA replication, we focused on the chromatin modification and transcriptional repression pathway. Notably, KAP1/TRIM28, one of the eleven proteins in this pathway (Figure 2E), was a surprising discovery at viral replication forks in light of its role in transcriptionally silencing viral lytic genes during the latent state. During the latent state, the constitutive heterochromatin machinery plays a key role in silencing viral lytic genes, thereby keeping EBV and other herpesviruses latent (21,25,49–56). KAP1 is a core constituent of this silencing machinery. Confirmatory iPOND-immunoblotting experiments demonstrated that KAP1 was indeed enriched at viral forks though only during active replication. KAP1 occupancy was lost if replication was blocked; KAP1 was also absent from newly replicated linear viral genomes (Figures 3A and B). With phosphorylation of KAP1 at S824 previously observed during the lytic phase (21), we examined viral forks and found that KAP1 at the forks was phosphorylated at S824 (Figures 3A and B). Furthermore, among cells lytically reactivated for 36 h, those with higher abundance of KAP1 were more likely to replicate the viral genome (Figure 3C). These experiments reveal that cellular proteins contributing to distinct functional pathways are recruited to actively replicating versus newly replicated viral genomes and further, a prominent transcriptional corepressor enriches with the viral replication machinery during the lytic phase.

KAP1 SUMOylates the viral DNA polymerase processivity factor during active replication

With KAP1, a SUMO2 ligase, occupying viral replication forks, we used a position frequency matrix-based scoring algorithm (57) and a group-based prediction algorithm (58) to identify viral replication proteins with putative SUMO target

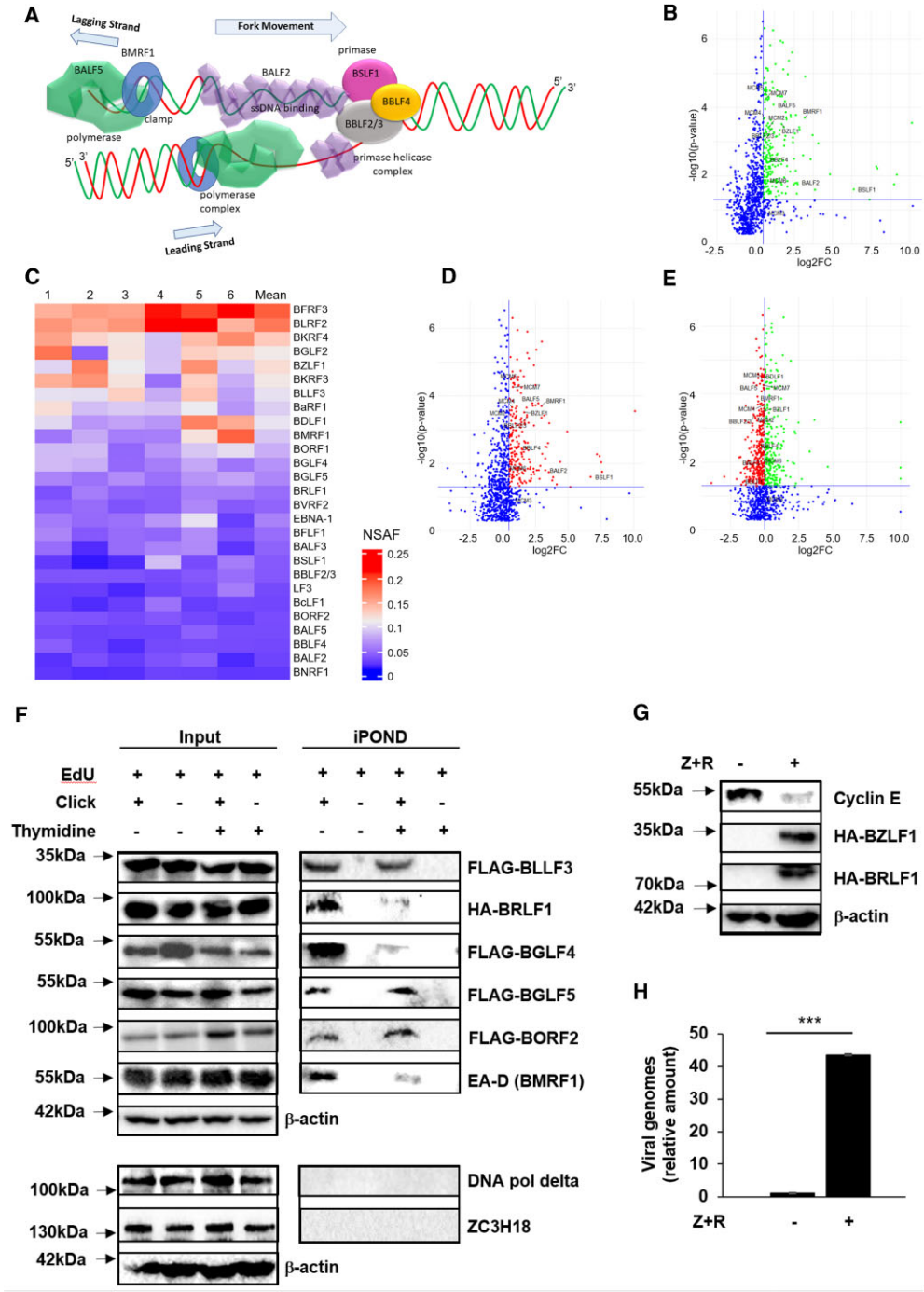

Figure 1. EBV proteins are enriched at viral DNA forks. (**A**) Schematic of the EBV replication fork. EBV genome replication during the lytic phase originates at one of two lytic origins of replication and requires a primase helicase complex comprised of a primase (BSLF1), primase-associated factors BBLF2 and BBLF3, and a helicase (BBLF4). BSLF1 synthesizes RNA primers that accumulate on the lagging strand for the initiation of DNA synthesis. The viral major DNA binding protein (BALF2) further unwinds DNA and stabilizes ssDNA within the replication fork while the DNA polymerase (BALF5) catalyzes the synthesis of new viral DNA in association with early antigen-diffuse (EA-D, BMRF1) which enhances the processivity of the polymerase complex. (**B–E**) EBV proteins identified by iPOND-mass spectrometry (MS). B shows a volcano plot of log2 fold change (log_2FC) versus $-log_{10}$ (*P*-value) for each protein enriched by iPOND. Green indicates proteins enriched in iPOND with $log_2FC > 0.5$ over background. Components of the cellular pre-replication complex (MCM2-7) and EBV DNA replication fork proteins are labeled. (**C**) Heat map of normalized spectral abundance factors (NSAF) for all viral proteins meeting the above cut-off are shown as the average of two technical replicates for each of six biological replicate samples as well as the overall mean (last column). (**D**) Volcano plot of log_2FC versus –log10 (*P*-value) for proteins enriched by iPOND in thymidine chase samples compared to background (red). (**E**) Volcano plot of the ratios of all significant proteins (*P*-value < 0.05) in viral iPOND samples to thymidine chase samples expressed as log2FC showing greater enrichment in viral iPOND samples (green) versus thymidine chase samples (red). (**F**) EBV proteins at replication forks using iPOND-immunoblotting; 293-EBV cells were transfected with HA-*BZLF1*, HA-*BRLF1* and FLAG-tagged EBV ORF plasmids for 36 h and pulsed with EdU for 20 min prior to harvest and iPOND for active forks (EdU). For isolating mature newly replicated viral DNA (Thymidine), EdU-labeled cells were washed with thymidine containing medium and then incubated with thymidine for 30 min prior to performing iPOND and immunoblotting. (**G, H**) 293-EBV cells were transfected with HA-*BZLF1* (Z) and HA-*BRLF1* (R) for 36 h and analyzed by immunoblotting (**G**) or qPCR to measure EBV genome replication; error bars, SEM (**H**). Experiments were performed three times.

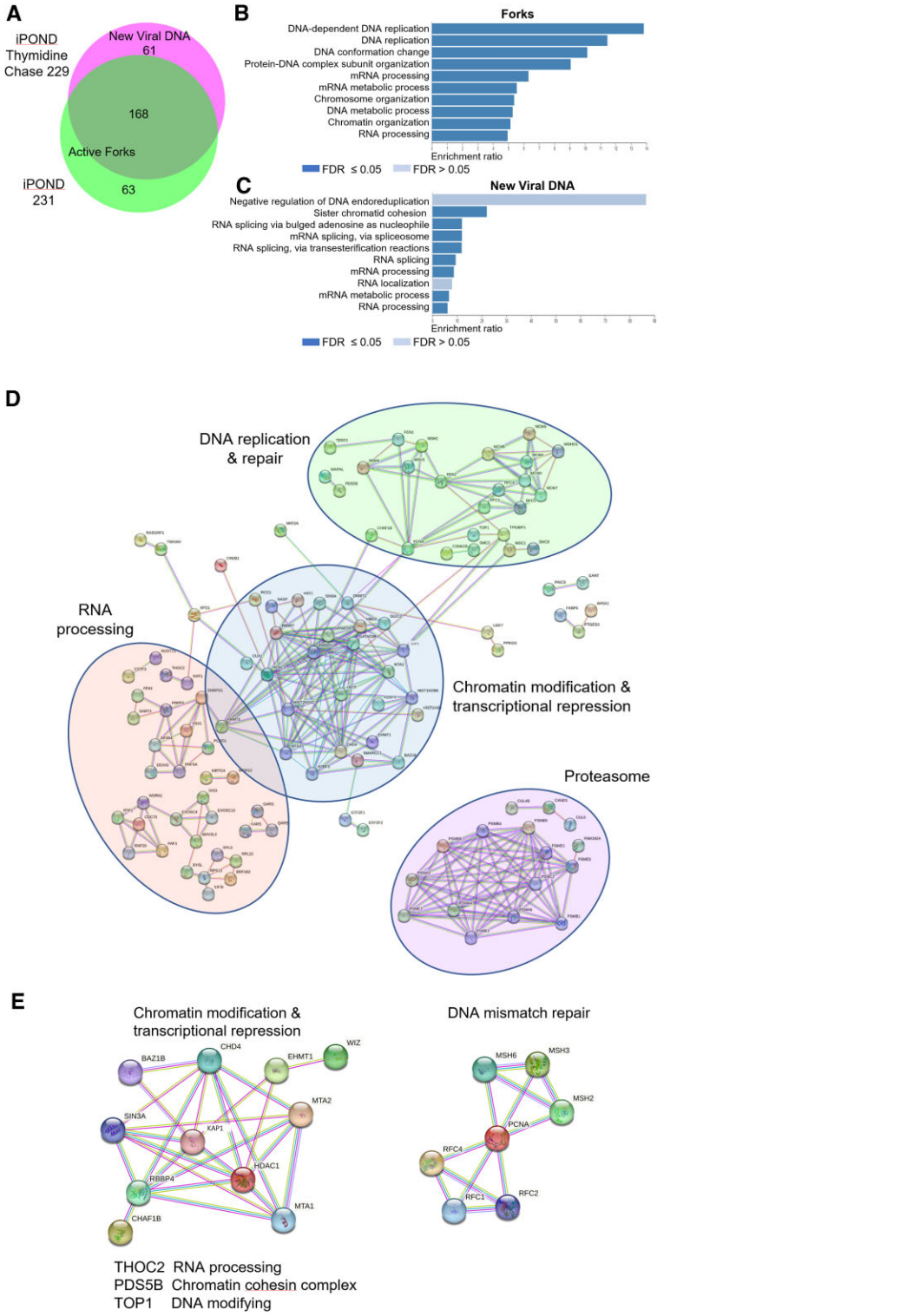

Figure 2. Pulse and pulse chase analysis showing cellular proteins at active viral forks and newly replicated linear viral genomes, respectively. (**A**) Normalized iPOND (231 proteins) and iPOND Thymidine chase (229 proteins) with *P*-values <0.05 and enriched over background (no click and PAA treated) by $\log_2$ fold change >0.5. Many active replication fork proteins (green, 231) overlapped with iPOND Thymidine chase proteins (168 proteins), while proteins associated with newly replicated linear viral DNA appeared exclusively in the iPOND Thymidine chase set (pink, 61 proteins). Statistically significant biological processes for Active Forks (**B**) versus New Viral DNA (**C**) were determined by overrepresentation analysis (ORA) and plotted according to the Enrichment ratio score for each gene set and biological process using WebGestalt 2019; FDR, false discovery rate. (**D**) Putative functional and physical interactomes of EBV iPOND enriched cellular proteins in the active forks dataset. Statistically significant EBV iPOND cellular proteins were subjected to STRING analysis to identify high confidence interactions (depicted). Functional pathways (circled) include DNA replication & repair, chromatin modification & transcriptional repression, RNA processing and proteasome. (**E**) Cross-analysis depicting putative functional and physical interactomes of 21 cellular proteins in common at EBV replication forks (from D) and the previously published nascent HSV-1 genome in an infection model (20). Edges (lines) in (D) and (E) indicate functional links or experimentally observed interactions (light green, text mining; cyan, database links; magenta, experimental evidence; purple, homology).

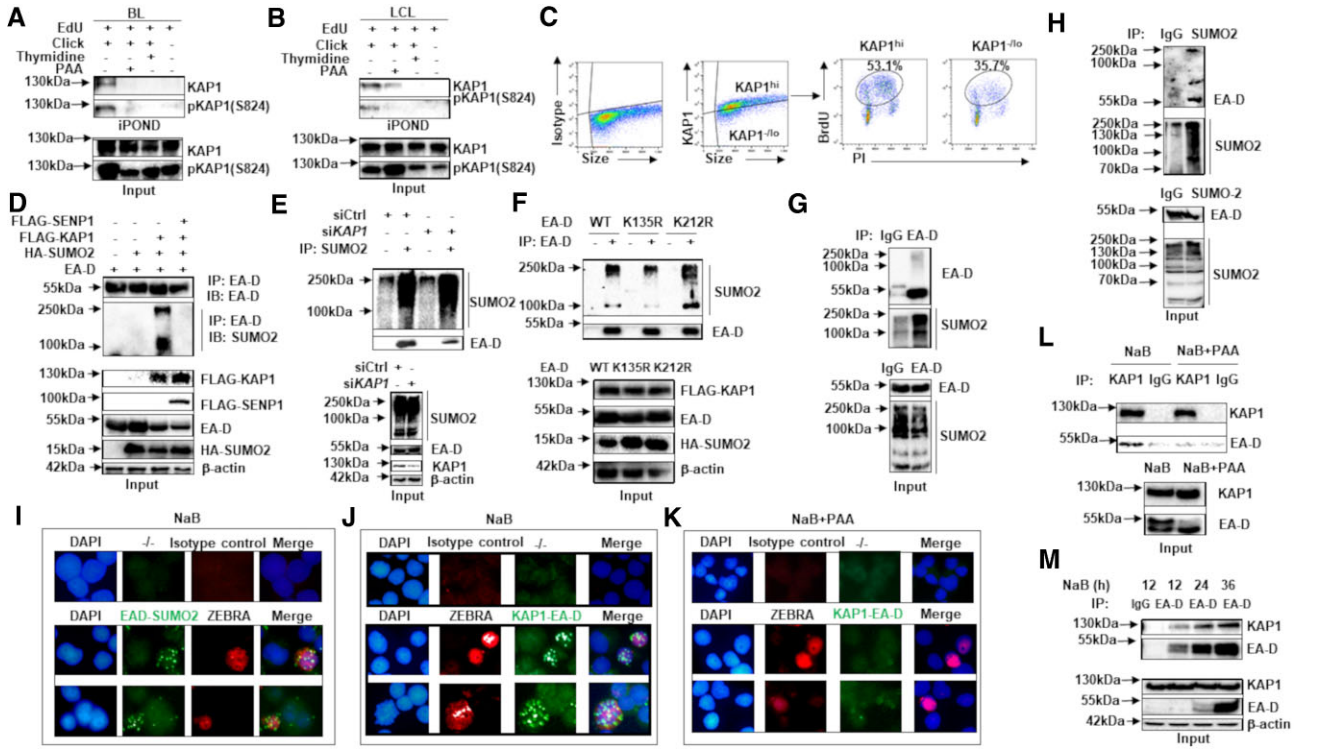

Figure 3. KAP1 conjugates SUMO2 to polymerase processivity factor EA-D at K135 during DNA replication. (**A, B**) BL cells (A) and LCL (B) were treated with NaB with or without PAA for 36 h and analyzed using iPOND for active forks (EdU) and mature newly replicated DNA (using thymidine) and immunoblotted with indicated antibodies. Click group was processed with biotin azide. (**C**) BL cells exposed to NaB for 36 h were then labeled with BrdU for 2 h. Harvested KAP1^{hi} and KAP1$^{-/lo}$ cells (left two panels) were assayed for BrdU uptake (right two panels) using flow cytometry. (**D**) HEK-293T cells were transfected with FLAG-*BMRF1* (EA-D), FLAG-KAP1, FLAG-SENP1 and HA-SUMO2. After 48 h, lysates were immunoprecipitated with anti-EA-D antibody prior to immunoblot analyses. (**E**) 293-EBV cells were co-transfected with siRNA targeting *KAP1* alongside FLAG-*BZLF1* and FLAG-*BRLF1* to reactivate EBV. After 36 h, lysates were immunoprecipitated with anti-SUMO2 antibody or control IgG and then immunoblotted. (**F**) HEK-293T cells were transfected with wild type FLAG-*BMRF1* (WT) or mutants (K135R, K212R) together with FLAG-KAP1 and HA-SUMO2 for 48 h. Lysates were immunoprecipitated with anti-EA-D antibody or control IgG and immunoblotted as indicated. (**G, H**) BL cells were treated with NaB for 24 h and lysates were immunoprecipitated with anti-EA-D antibody versus control IgG (G) or anti-SUMO2 antibody versus control IgG (H), and then immunoblotted as indicated. (**I–K**) To assess proximity by proximity ligation assay (PLA), LCL were exposed to NaB without (I, J) or with (K) the addition of PAA for 36 h; lytic cells were marked using an anti-ZEBRA antibody. (**L**) LCL were exposed to NaB with or without the addition of PAA for 36 h prior to immunoprecipitation using an anti-KAP1 antibody or control IgG followed by immunoblotting. (**M**) BL cells were exposed to NaB for different lengths of time prior to immunoprecipitation with anti-EA-D antibody versus control IgG and then immunoblotted. Experiments were performed three times.

sites. Of EBV replication proteins predicted to be SUMOylated by both algorithms (Table S3), the viral DNA polymerase processivity factor EA-D emerged as the top candidate with two predicted SUMO sites (K135 and K212). We found EA-D to be abundantly SUMO(2)ylated only when we expressed EA-D with KAP1 (Supplementary Figure 3D and S3); notably, EA-D lost its SUMOylation when a SUMO peptidase (SENP1) was co-expressed (Figure 3D) or when KAP1 was depleted, apparent by less pull down of EA-D with anti-SUMO2 antibody in siKAP1 versus siCtrl conditions (Figure 3E). Further, EA-D lost KAP1-mediated SUMOylation when K135, the first of the two predicted SUMO sites, was mutated but not when K212 was mutated, implicating K135 as the relevant SUMO2 target site on EA-D (Figure 3F). Examination of endogenous EA-D also revealed SUMO2 (Figures 3G and H) but not SUMO1 (Supplementary Figure S4) modification in cell extracts of lytically activated BL cells.

Since KAP1 was needed for SUMOylation of EA-D, we investigated the topologic relationship between KAP1 and EA-D using proximity ligation assay (PLA), an in-situ assay that yields a fluorescent focus when two proteins of interest are within 40 nm of each other (59). We found that in lytically activated cells, KAP1 and EA-D were adjacent and most notably, PLA signals were lost when the viral DNA polymerase was inhibited using PAA (Supplementary Figure 3I, J, K, Supplementary Figure S5A and B). These results were further supported by co-precipitation of KAP1 and EA-D only when the viral DNA polymerase was functional (Supplementary Figure 3L and S5C). Additionally, KAP1-EA-D co-enrichment became more prominent with progress of the lytic phase (Figure 3M). These results implicate KAP1 in SUMO2 ligation at K135 of EA-D during active viral DNA replication.

Transcription-dependent phosphorylation of KAP1 and its recruitment to the replication machinery results in SUMOylation of EA-D and viral fork stability.

KAP1 has been implicated in SUMOylating the cellular DNA polymerase processivity factor PCNA, resulting in avoidance of collisions between transcription and replication machineries (60,61). To address if KAP1 was functioning in a similar manner to cause transition from transcription to replication of the viral genome, we examined the effects of transiently blocking transcription ∼24 h post reactivation, i.e. when the viral genome is known to have adequately transcribed

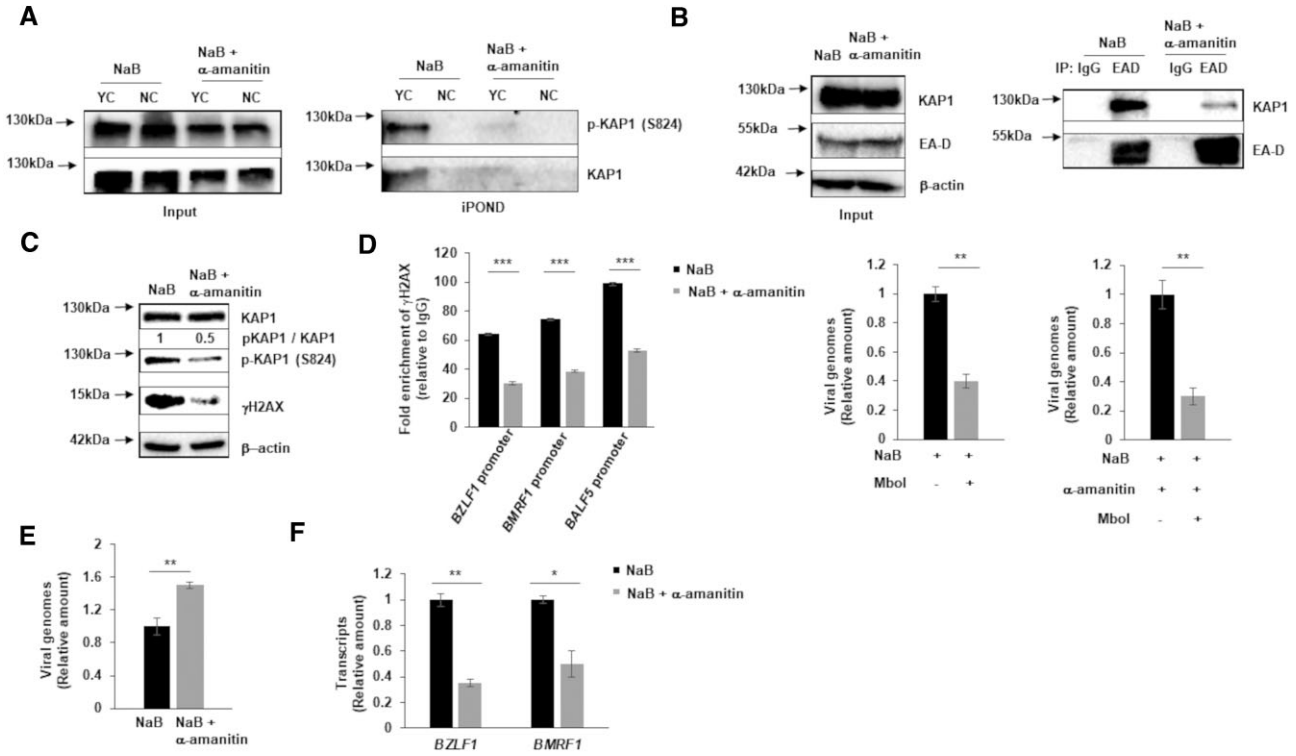

Figure 4. Recruitment of KAP1 to EA-D at replication forks requires transcription. (**A**) BL cells were exposed to NaB for 30h with α-amanitin added for the last 6h. Cells were then harvested for iPOND followed by immunoblotting. YC, yes click group, processed with biotin azide; NC, no click control group, processed without biotin azide. (**B, C, E, F**) EBV in BL cells was reactivated using NaB for 24 h while blocking transcription using α-amanitin for the last 6 h. Cells were harvested for immunoprecipitation with anti-EA-D antibody (versus IgG as control; (B), immunoblotting (C), quantitation of viral genomes by qPCR (E) and quantitation of immediate early and early gene transcripts via RT-qPCR (F). In panel **D**, BL cells were exposed to NaB for 30 h with α-amanitin added for the last 6h. DNA was precipitated using antibody to γH2AX and exposed to MboI to digest newly replicated non-methylated DNA. Primer pairs spanning MboI sites were used to amplify indicated loci on episomal genomes using qPCR. Efficiency of MboI digestion was assayed by qPCR using a pair of primers spanning an MboI site on the *BALF5* gene (middle and right-hand side panels). Error bars, SEM of three technical replicates. Experiments were performed twice.

immediate early and early genes and transitions to replicating its genome (Supplementary Figure S2). Transient (i.e. 6 h) exposure to α-amanitin that selectively degrades the largest subunit of RNA polymerase II (RPOII) and greatly reduces the rate of transcription (62,63), resulted in loss of recruitment of KAP1 and S824 phospho-KAP1 to viral forks (Figure 4A). This absence of KAP1 at the forks correlated with reduced interaction between KAP1 and EA-D (Figure 4B). Notably also, blocking transcription impaired phosphorylation of KAP1 as well as phosphorylation of the histone H2AX (i.e. γH2AX), the double-strand DNA break sensor (Figure 4C). Importantly, blocking transcription reduced DNA lesions on the viral genome as demonstrated by reduced enrichment of γH2AX at several viral loci (Figure 4D); in this experiment, newly replicated linear viral genomes were digested using MboI, a methylation sensitive restriction endonuclease, ensuring PCR amplification of only parental/episomal genomes (Figure 4D). Transiently inhibiting transcription not only reduced damage to DNA but also increased replication of the viral genome (Figure 4E). As expected, the inhibitor impaired transcription of *BZLF1* and *BMRF1* (Figure 4F). Thus, while transcription was needed for KAP1 phosphorylation, its recruitment to replication forks and KAP1–EA-D interaction, transiently slowing transcription reduced DNA damage and amplified viral genome replication. Remarkably also, following the start of DNA replication (~18–24 h), the abundance of EA-D protein was no longer highly reliant on active translation; indeed, EA-D protein seemed stable enough to withstand a temporary inhibition of transcription (Figures 4B, F).

To assess the effects of KAP1-mediated EA-D SUMOylation on viral genome replication, we reactivated EBV by introducing *BZLF1* and *BRLF1* into cells carrying an EA-D/*BMRF1*-deleted EBV bacmid (B072-1 cells). Compared to cells in which wild type EA-D or K212R EA-D mutant was provided, cells expressing K135R EA-D demonstrated significantly less viral genomes, highlighting the importance of SUMOylation of EA-D in DNA replication (Figure 5A). Importantly, DNA fiber fluorography revealed that depletion of KAP1 resulted in fewer and shorter replication forks (Figures 5B-D)—this could result from firing of fewer origins or from collapse of replication forks. Lytic replication is thought to occur predominantly by rolling circle replication from the lytic origin of replication (oriLyt), of which only up to two exist in the EBV genome (64); this is in contrast to replication of the host genome which occurs from many origins of replication. In support of collapsed replication forks, depletion of KAP1 or impaired K135 SUMOylation of EA-D resulted in greater DNA damage demonstrated by increased γH2AX (Figures 5E and 5F), likely from interference between the replication and transcription machineries—recall that temporary slowing of transcription (after early gene products were abundant) resulted in reduced DNA damage and increased viral genome copies (Figures 4C–E).

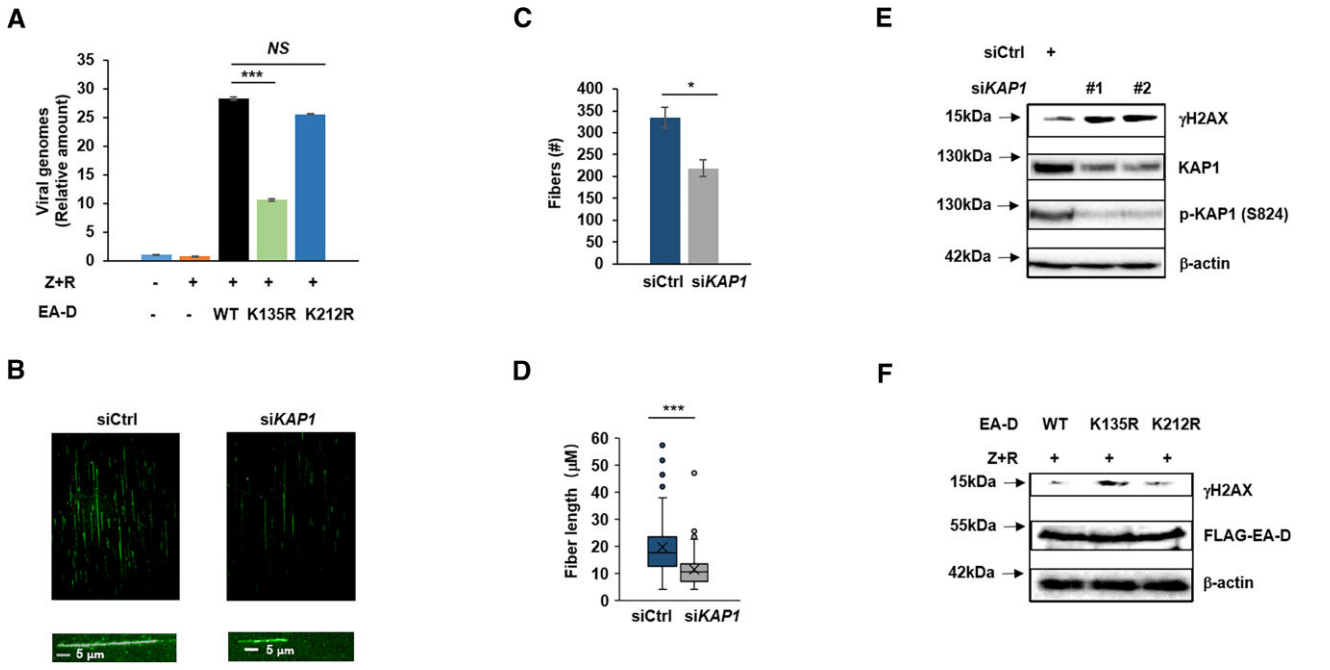

Figure 5. KAP1 mediated SUMOylation of EA-D stabilizes viral DNA replication forks. (**A**) EA-D/*BMRF1*-deleted EBV bacmid-carrying 293-EBV (B072-1) cells were transfected with wild type FLAG-*BMRF1* (WT) or mutants (K135R, K212R) together with FLAG-*BZLF1* and FLAG-*BRLF1* to reactivate EBV. After 36 h, viral genomes were quantified via qPCR. (B–E) 293-EBV cells were transfected with si*KAP1* (versus siCtrl) and FLAG-*BZLF1* and FLAG-*BRLF1* for 36 h and extracted DNA subjected to DNA fiber fluorography (**B–D**) or lysates immunoblotted with indicated antibodies (**E**). Representative images from DNA fiber analysis (B), fiber counts (C) and cumulative data including median value of track/fiber length from at least 150 tracks per experimental condition (D) are shown. $*P < 0.05$, $***P < 0.001$. (**F**) *BMRF1*-KO 293-EBV cells were transfected with wild type FLAG-*BMRF1* (WT) or mutants (K135R, K212R) together with FLAG-*BZLF1* and FLAG-*BRLF1* plasmids for 36 h prior to performing immunoblotting. Experiments were performed at least twice. Error bars in (A), SEM of three technical replicates.

Of note, depletion of PCNA, the cellular homolog of EA-D, had no effect on the abundance of newly replicated viral genomes (Supplementary Figure S6). While some have found PCNA to be excluded from replication complexes, others have implicated PCNA in mismatch repair-mediated maturation of newly synthesized viral DNA; neither of these scenarios link PCNA to viral genome replication per se (65–67). In summary, transcription-dependent phosphorylation and recruitment of KAP1 to the replication machinery is important for viral genome replication, and the absence of these activities results in replication fork collapse, thereby functionally linking transcription to replication of the episomal genome.

The PI3KK ATM and the RNA polymerase II associated helicase RECQ5 collaborate to recruit and phosphorylate KAP1, resulting in SUMOylation of EA-D.

The RPOII-associated DNA helicase RECQ5 has been linked to KAP1-mediated SUMOylation of PCNA. SUMOylation of PCNA, the cellular homolog of EA-D, averts transcription-replication collisions in the cell (60,61). To address the mechanics of KAP1 activation, we depleted RECQ5 and found that phosphorylation of KAP1, co-enrichment between KAP1 and EA-D, and SUMOylation of EA-D were impaired (Supplementary Figure S7A–C). Importantly, depletion of RECQ5 also dampened viral genome replication and transcription of *BZLF1* and *BMRF1* (Supplementary Figure S7D-F)—likely secondary to interference between the transcription and replication machineries supported also by the observations that depleting KAP1 and replacing wild type EA-D with the K135R mutant resulted in replication fork damage (Figures 5B–F). While loss of abundance of *BZLF1* and *BMRF1* transcripts upon RECQ5 depletion in Supplementary Figure S7E could be due to impaired function of RPOII, this is unlikely as several studies have shown that RECQ5 inhibits transcription elongation by RPOII, thereby reducing transcription stress (68–70). Thus, taken together with the results in Figures 4 and 5, the drop in DNA replication and immediate early and early transcripts upon RECQ5 depletion (in Supplementary Figure S7) are due to conflicts resulting from simultaneous transcription and replication from the episomal genomes.

Our earlier studies had identified the PI3 kinase related kinase ATM as the kinase that phosphorylates KAP1 at S824 during the lytic phase (21). Indeed, we found that the ATM inhibitor KU55933 not only blocked KAP1 phosphorylation but also impaired SUMOylation of EA-D (Figures 6A and B). Depletion of ATM similarly impaired KAP1 phosphorylation as well as the interaction between phospho-KAP1 and RECQ5 (Figure 6C). Depletion of ATM also resulted in impaired precipitation of RPOII and RECQ5 by KAP1 (Figure 6D)—placing KAP1 and phospho-KAP1 at the transcription machinery with RECQ5. Together, these results support a role for ATM in recruitment and phosphorylation of KAP1 in the context of the transcription machinery.

SUMOylation of EA-D reinstates heterochromatin via the histone methyltransferase SETDB1 to prioritize replication of the viral genome.

Given our observations on transcription-dependent and ATM-RECQ5-mediated phosphorylation and recruitment of

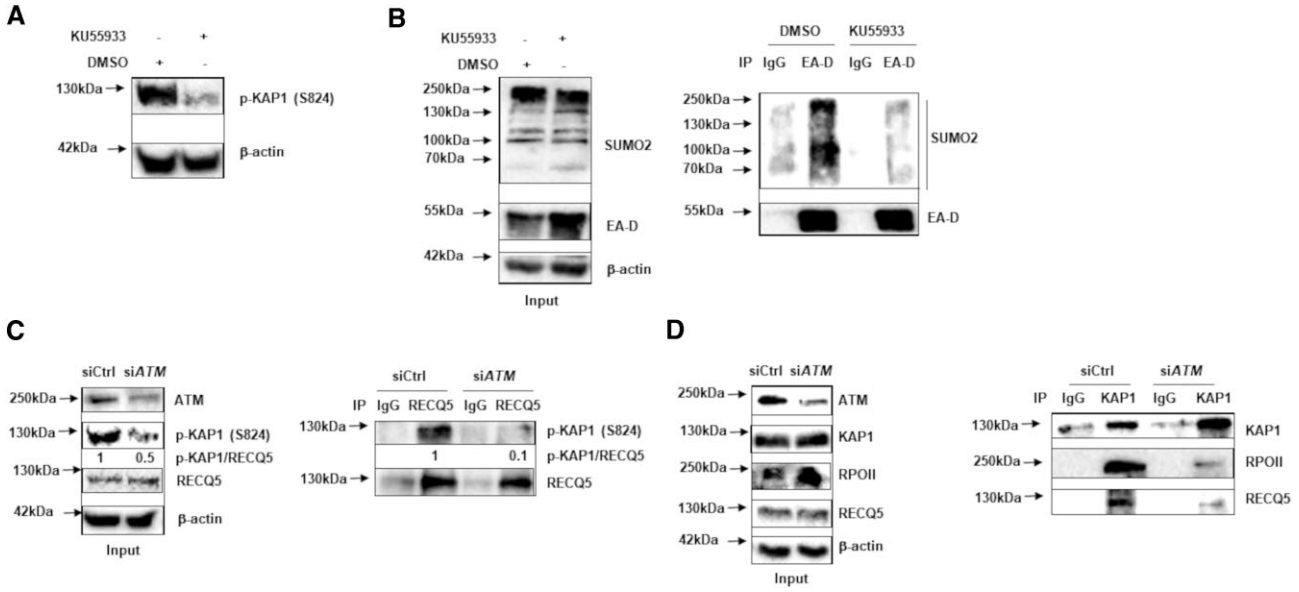

Figure 6. The PI3KK ATM recruits and phosphorylates KAP1 at the RPOII-RECQ5 complex. (**A, B**) BL cells were treated with NaB with or without the ATM inhibitor KU55933 for 24 h. Cells were harvested for immunoblotting (A) or immunoprecipitation with anti-EA-D antibody or control IgG (B). (**C, D**) BL cells were transfected with si*ATM* or scrambled siRNA (siCtrl) for 20 h followed by exposure to NaB for 24 h. Lysates were immunoprecipitated with anti-RECQ5 antibody (C) or anti-KAP1 antibody (D) and then immunoblotted using indicated antibodies. Experiments were performed twice.

KAP1 to the replication machinery, and as a result, SUMOylation of EA-D, as well as identification of CAF1B/CHAF1B at forks by iPOND-MS (Figure 2D), we depleted RECQ5 and immunoprecipitated the largest of the three components of the chromatin assembly factor CAF1 (CAF1A), the histone variant H3.1, and the silencing histone mark H3K9me3. After digesting linear i.e. newly replicated viral genomes using MboI, we PCR amplified immediate early and early lytic promoters and gene bodies from the parental/episomal genomes. Following DNA replication, the histone chaperone CAF1 typically deposits histones including the repressive H3.1 to re-establish repressive H3K9me3 chromatin marks (71–74). Figure 7A–D shows that depletion of RECQ5 resulted in reduced occupancy by CAF1A, H3.1 and H3K9me3 on episomes, indicating that RECQ5-orchestrated SUMOylation of EA-D results in restriction of transcription from episomal viral genomes via chromatin remodeling; in comparison, the occupancy of H3K4me3 and H3K9acetyl activation marks remained unchanged in response to RECQ5 depletion (Supplementary Figure S8). In further support, Figures 7E, F, I demonstrate that SUMOylated EA-D interacted with CAF1A but lost this ability when RECQ5 was depleted or the K135R mutant EA-D was expressed. Furthermore, depletion of RECQ5 resulted in increased γH2AX when ATM was ectopically expressed (Figure 7H). These results, together with (i) the data showing that transcription is necessary for phosphorylation of H2AX (Figures 4C, D), (ii) that lack of KAP1 and lack of SUMOylation of EA-D increase DNA damage (sensed by γH2AX; Figure 5B–F) and (iii) with RECQ5 known to prevent transcription-replication collisions (60,61), further support the idea that ATM, RECQ5, KAP1 and EA-D collaborate to dampen transcription from the episome, thereby preventing interference between the transcription and replication machineries and allowing replication to continue. This is further supported by the observation that depletion of RECQ5, dampens instead of increasing transcription from the episomal genome (measured by nascent transcripts of *BZLF1* and *BMRF1* in Figure 7G); RECQ5 is known to inhibit transcription elongation by RPOII (68–70). This reduction in transcription in the face of RECQ5 unavailability is likely due to continued transcription and the resulting interference with the replication machinery. However, the presence of DNA damage resulting from RECQ5 depletion is only sensed (i.e. phosphorylation of H2AX) when ATM is exogenously provided, suggesting an additional role for RECQ5 in recruiting ATM to the transcription machinery (Figure 7H); ATM is known to phosphorylate H2AX in response to DNA lesions.

Of the five known histone 3 lysine 9 methyltransferases (EHMT1, EHMT2, Suv39h1, Suv39h2 and SETDB1) potentially recruited to silence the episome, we found that only SETDB1 coprecipitated with CAF1A when RECQ5 was abundant (Supplementary Figure S9). Moreover, like depletion of RECQ5, depletion of SETDB1 resulted in reduced enrichment of H3K9me3 marks on episomal viral genomes (Supplementary Figure S10A–C) and dampened viral genome replication (Supplementary Figure S10B, minus MboI conditions). Thus, RECQ5 directs CAF1 to recruit SETDB1 to the replication machinery. Although EHMT1/GLP1 was identified by iPOND-MS (Figure 2D), we were unable to detect it in a CAF1A complex. That said, KAP1, CAF1 and SIN3A, all identified by our iPOND-MS, are known to interact with SETDB1, supporting its enrichment in a CAF1A complex.

Thus, the coordinated efforts of the cellular transcription machinery, the viral DNA polymerase processivity factor, and a set of cellular enzymes (a helicase, a kinase, a SUMO2-ligase and a histone methyl transferase) restrict viral transcription from the episomal template to prioritize genome replication. We believe this results in the handover from transcription to replication of the episome during the lytic phase of EBV.

Discussion

Human herpesviruses are responsible for infecting the entire human population, with EBV alone infecting and

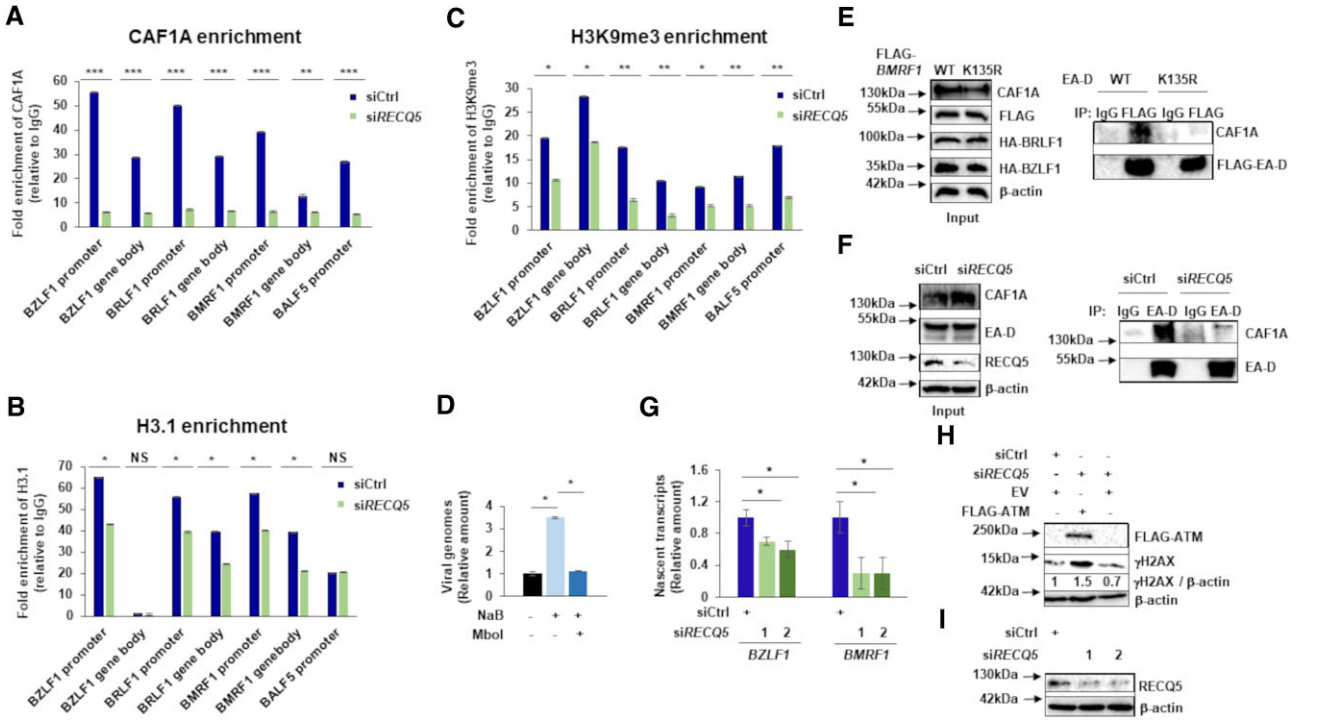

Figure 7. RECQ5 facilitates EA-D-mediated recruitment of silencing histones to the episomal EBV genome. (**A–D**) BL cells were transfected with si*RECQ5* or scrambled siRNA (siCtrl) for 20h followed by treatment with NaB for 24h. Nuclei were subjected to chromatin immunoprecipitation with anti-CAF1A antibody (A), anti-Histone H3.1 antibody (B) and anti-H3K9me3 antibody (C). Precipitated DNA was exposed to MboI to digest newly replicated non-methylated DNA. Primer pairs spanning MboI sites were used to amplify indicated loci on episomal genomes using qPCR in A-C. Fold enrichment of CAF1A, H3.1 and H3K9me3 on DNA was analyzed after normalizing to control IgG pull down. Efficiency of MboI was assayed by qPCR using a pair of primers spanning an MboI site on the *BALF5* gene (D). (**E**) EA-D/*BMRF1*-deleted EBV bacmid-carrying 293-EBV (B072-1) cells were transfected with wild type (WT) or mutant (K135R) FLAG-*BMRF1* together with HA-*BZLF1* and HA-*BRLF1* for 36 h prior to immunoprecipitation with an anti-FLAG antibody. (**F**) BL cells were transfected with si*RECQ5* or scrambled siRNA (siCtrl) for 20 h followed by treatment with NaB for 24h prior to immunoprecipitation with an anti-EA-D antibody. (**G, I**) BL cells were transfected with si*RECQ5* or scrambled siRNA (siCtrl) for 20 h followed by exposure to NaB for 24 h and subjected to BrU-RT-qPCR analysis to measure nascent *BZLF1* and *BMRF1* transcripts (G) or immunoblotting (I). (**H**) BL cells were transfected with empty vector (EV), FLAG-ATM plasmid, si*RECQ5*, or scrambled siRNA (siCtrl) for 20 h followed by treatment with NaB for 24 h before immunoblotting with indicated antibodies. Error bars, SEM of three technical replicates. These experiments were performed at least twice.

remaining dormant in ∼95% of humans. Indeed, collectively herpesviruses contribute to significant disease burden that is mostly associated with their replicative phase. Understanding the mechanisms that govern their replication is thus essential to developing therapies against herpesvirus diseases. Unlike most other herpesviruses though, EBV also contributes to several types of cancer with the lytic phase playing an important role (75). With efficient and accurate replication of the viral genome central to their life cycle, herpesviruses encode the core components of the replication machinery, thereby maintaining autonomy over their ability to replicate their genomes. That said, to successfully propagate and spread, viruses also effectively exploit host biology including mechanisms of chromatin remodeling that regulate important processes such as silencing pericentromeric regions and endogenous retroviral elements, influencing genome stability and gene expression, and maintaining heritable epigenomes (76–79). Our study demonstrates that invaders like EBV coopt such epigenetic regulators, and together with other cellular and viral factors, tightly regulate the temporal order of events during the virus's replicative phase—this directional control strictly enforcing early gene transcription followed by replication of viral genomes is essential for virus production and represents a central theme among DNA viruses (80–83). Our findings also highlight the dynamic nature of epigenetic regulation of the viral genome. Herpesvirus genomes are chromatinized during the latent state, and while several studies indicate that silencing marks need to be removed to disrupt latency and transcribe immediate early and early lytic genes (25,49,84–86), results presented here highlight the importance of reinstating such marks for transition from transcription to genome replication.

EBV's restriction of early gene transcription to enable viral replication represents a hybrid model that is reminiscent of aspects of cellular mechanisms that a) avoid transcription-replication interference and b) re-chromatinize newly replicated host genomes. Transcription-replication interference (a, above) occurs frequently in regions of the cell genome (e.g. common fragile sites) that are heavily transcribed during the S phase of the cell cycle. This situation is analogous to the herpesvirus lytic phase in which the viral genome, tightly packed with ORFs, is transcribed heavily as replication begins. To avoid collisions between the transcription and replication machineries at fragile sites, the RPOII-associated DNA helicase RECQ5, through mechanisms that are not known, activates KAP1 resulting in SUMOylation of PCNA; as a result, CAF1 and H3.1 are recruited to block transcription (60,61). To maintain heterochromatin signatures through cell division (b, above), KAP1, through an unknown kinase, is phosphorylated at S473 which prompts its interaction with PCNA

and the H3K9 trimethyl transferase Suv39h1, resulting in H3K9me3 marks on select portions of the newly replicated cell genome (87). In the hybrid scenario, to facilitate transition to DNA replication, EBV enlists ATM, which in the presence of RECQ5 at the transcription machinery, recruits and phosphorylates KAP1 at S824. Phospho-KAP1 then ligates SUMO2 at K135 of EA-D, the viral homolog of PCNA. This results in recruitment of CAF1, H3.1 and the H3K9 mono, di, and trimethyltransferase SETDB1. This mechanistic model also provides topological information in that ATM-mediated phosphorylation of KAP1 occurs in the context of the transcription machinery (supported by immunoprecipitation experiments with RPOII) but phospho-KAP1-mediated SUMOylation of EA-D occurs at viral replication forks (supported by enrichment of phospho-KAP1 and EA-D at replication forks, and loss of interaction between KAP1 and EA-D in the presence of PAA). A notable distinction from (b) above is that while KAP1, phosphorylated at S473, cooperates with Suv39h1 to reinstate heterochromatin on newly replicated cellular genomes, in the context of viral replication, KAP1, phosphorylated at S824, collaborates with SETDB1 to instead reinstate heterochromatin on parental viral genomes that serve as templates for replication. Notably also, lytic cells lack S473-phosphoKAP1 but have S824-phosphoKAP1, an observation we previously made (21); absence of S473-phosphoKAP1 also likely ensures that newly replicated viral genomes are left unchromatinized and thus able to serve as templates for transcription of late genes. In earlier work, we had also demonstrated that the viral protein kinase (vPK, *BGLF4* product) phosphorylates/activates ATM (51). The presence of vPK at viral replication forks in the present study (Figure 1F) implicates vPK's proximity to the transcription machinery as a likely trigger for ATM phosphorylation and KAP1 recruitment.

While the model above describes how EBV orchestrates the handover from transcription to replication, we also identified two viral proteins, not previously linked to EBV replication, enriched on nascent viral DNA that additionally support this handover. The first is the large subunit of the ribonucleotide reductase (RNR; encoded by *BORF2*), an enzyme that converts nucleotides to deoxynucleotides, maintaining a supply of dNTPs during DNA synthesis. The other is the viral *BLLF3*-encoded dUTPase, a hydrolase that converts dUTP to dUMP, ensuring availability of a substrate for thymine nucleotide synthesis. By shifting the balance from RNA substrates to DNA substrates at replication forks, these two enzymes likely aid the shift from transcription to replication that is spearheaded by ATM, KAP1 and EA-D. The presence of RNR and dUTPase at forks may also restrict errors in viral DNA replication. Limiting the amount of dUTP at forks keeps misincorporation of uracil into DNA and the resulting error prone uracil glycosylase-mediated excision repair to a minimum. Furthermore, the *BORF2* gene product has been shown to contribute to viral genome integrity by neutralizing cellular APOBEC3B (88). We suspect that using EdU for iPOND enabled detection of the two viral enzymes at forks; notably, they were not detected by another iPOND-MS study in an infection model that used a mutant HSV-1 lacking both enzymes (20). The possibility of cellular orthologs of viral RNR and dUTPase similarly traveling with the human DNA replication machinery to limit errors in genome replication particularly in cancer cells is intriguing.

Our iPOND-proteomic study of viral lytic forks yielded a few key findings. First, newly replicated virus genomes predominantly attracted proteins related to RNA metabolism, a finding consistent with the earlier observation that linear newly replicated viral genomes serve as templates for late gene transcription (48). Second, replication forks ∼36h after lytic activation engaged proteins involved in DNA replication and repair, RNA processing, the proteasome and remarkably, chromatin remodeling and transcription repression. Of these pathways, DNA mismatch repair and chromatin remodeling/transcriptional repression pathways were in common with a study of proteins at HSV-1 replication forks (20). Within the chromatin remodeling/transcriptional repression pathway, were HDAC proteins involved in gene silencing, KAP1 that recruits the H3K9MT SETDB1, subunits of CAF1 that recruit SETDB1 & silencing histones such as H3.1, the H3K9MT GLP/EHMT1, a zinc finger protein (WIZ) that contributes to EHMT1-EHMT2 dimerization, and the HDAC subunit SIN3A that interacts with SETDB1 (87,89–91). Notably, in support of several of the above replication fork-enriched proteins informatically pointing to SETDB1, our experiments identified SETDB1 as the only H3K9MT complexed with CAF1 when RECQ5 was abundant. As for KAP1, we and others had previously established KAP1 as an essential pro-latent factor for herpesviruses (21,25,49–56), and while KAP1 had been found to tether the replication machinery to EBV's lytic origin (92), its precise function during the lytic phase remained unclear. With KAP1 also identified at HSV-1 lytic forks (20), KAP1 may play a similar pro-lytic role in transcription-to-replication transition of other herpesviruses.

Of cellular replication and repair proteins identified at forks in our study, some (TOP1, CSNK2B) are known to contribute to viral DNA replication or repair during the lytic phase (93–95) while many others to our knowledge (TRF2, WAPAL, PDS5B, RFC1, RFC2, RC4) are not. Curiously, a recent study found that SMC5/6 interacts with R-loops at the EBV OriLyt to suppress the formation of replication compartments and that SMC5/6 must be degraded by a structural/late lytic viral protein (96), and yet, we found SMC6 at forks; the implications of SMC6 (and SMC2) at forks remains unclear. Although phosphorylation of MCM4 (in MCM4-6-7 complexes) by EBV vPK has been shown to impair its helicase function and therefore, block cellular DNA replication during the lytic phase (97), identification of MCM2, 4, 5, 6 and 7 at viral forks suggests a helicase-unrelated function. With EBV utilizing homologous recombination (HR) repair during the lytic phase (98), it is not surprising that several HR proteins were identified at lytic forks. Similarly, the base excision repair protein FEN1, several mismatch repair proteins (MSH2, 3 and 6) as well as PCNA, known to contribute to DNA repair and variably identified at viral replication compartments in other studies (65,99), were also identified in our study. That said, PCNA did not contribute to viral DNA amplification in our study, supporting a role in maturation of newly synthesized viral DNA as has been suggested by others (65–67). Likewise, enrichment of proteasome-related proteins likely contributes to fine tuning the abundance of replication proteins known to be important for faithful DNA replication (100).

In earlier work, we had demonstrated that very soon after lytic cycle induction (by ∼8 h), KAP1 is phosphorylated by ATM to depress heterochromatinized lytic genes on the

viral episome (21). While our present work indicates that phospho-KAP1 is important also for transitioning to DNA replication, this does not contradict our earlier findings as they represent functions at different stages of the lytic cycle—the contribution of KAP1 to transcription-replication handover occurs 24–36 hours after lytic cycle induction. Because the replication machinery is absent from the episome at early times (when transcription peaks), there is no EA-D on the forks for phospho-KAP1 to SUMOylate. Importantly, whether ATM, which phosphorylates KAP1 in EBV-infected cells and is known to also phosphorylate KAP1 in uninfected cells (101), participates in avoidance of transcription-replication collisions on cellular genomes remains to be seen.

With no anti-EBV agents or vaccines currently available, delineating mechanisms that are central to the virus's ability to replicate itself is key to discovering molecular nodes of intervention. These discoveries should guide further investigations into questions related to EA-D's recruitment of CAF1A and the roles that EA-D SUMOylation and potentially other modifications might play. While these investigations are likely to reveal novel aspects of cellular genome replication through mechanistic parallels between viral and cellular replicative processes, any divergence will be potentially exploitable for therapeutic gains.

Data availability

The mass spectrometry raw data files underlying this article are available in the ProteomeXchange Consortium via the MassIVE partner repository at https://massive.ucsd.edu/ProteoSAFe/static/massive.jsp, and can be accessed with the accession code MSV000091375.

Supplementary data

Supplementary Data are available at NAR Online.

Acknowledgements

We thank Dr Kathy Shair for sharing vectors encoding several EBV ORFs, Dr Lori Frappier for sharing a vector encoding the EBV BORF2 ORF, and Professor Kum Kum Khanna for sharing a plasmid encoding KAP1. We also thank Professor Henri-Jacques Delecluse for sharing the *BMRF1* knockout 293-EBV (B072-(1) cell line and Professor Paul Farrell for sharing the BZ1 antibody. We thank Dr Scott Tibbetts, Dr Beth Rousseau and Griffin Willman for constructive discussion.

Funding

Children's Miracle Network and NIH [R01 AI113134, U01 CA275310 to S.B.M.]; M.M. was supported by funds from the Children's Miracle Network, NIH [U01 CA275310]; DHS [70 RSAT 19 CB 0000027]. Funding for open access charge: Children's Miracle Network.

Conflict of interest statement

None declared.

References

1. Damania,B., Kenney,S.C. and Raab-Traub,N. (2022) Epstein–Barr virus: biology and clinical disease. *Cell*, **185**, 3652–3670.
2. Chakravorty,A., Sugden,B. and Johannsen,E.C. (2019) An epigenetic journey: Epstein-Barr virus transcribes chromatinized and subsequently unchromatinized templates during its lytic cycle. *J. Virol.*, **93**, e02247-18.
3. Farrell,P.J. (2019) Epstein–Barr virus and cancer. *Annu Rev Pathol*, **14**, 29–53.
4. Soldan,S.S. and Lieberman,P.M. (2023) Epstein–Barr virus and multiple sclerosis. *Nat. Rev. Micro.*, **21**, 51–64.
5. Kenney,S.C. and Mertz,J.E. (2014) Regulation of the latent-lytic switch in Epstein–Barr virus. *Semin. Cancer Biol.*, **26**, 60–68.
6. Burton,E.M., Goldbach-Mansky,R. and Bhaduri-McIntosh,S. (2020) A promiscuous inflammasome sparks replication of a common tumor virus. *Proc. Natl. Acad. Sci. U.S.A.*, **117**, 1722–1730.
7. Buschle,A. and Hammerschmidt,W. (2020) Epigenetic lifestyle of Epstein–Barr virus. *Semin. Immunopathol.*, **42**, 131–142.
8. Tsurumi,T. (2001) EBV replication enzymes. *Curr. Top. Microbiol. Immunol.*, **258**, 65–87.
9. Hammerschmidt,W. and Sugden,B. (2013) Replication of Epstein–Barr viral DNA. *Cold Spring Harb. Perspect. Biol.*, **5**, a013029.
10. Amen,M.A. and Griffiths,A. (2011) Packaging of non-coding RNAs into herpesvirus virions: comparisons to coding RNAs. *Front. Genet.*, **2**, 81.
11. Pellett,P.E. and Roizman,B. (2007) In: *The family of Herpesviridae: A Brief Introduction*. Lippincott-Williams and Wilkins, NY.
12. Lehman,I.R. and Boehmer,P.E. (1999) Replication of herpes simplex virus DNA. *J. Biol. Chem.*, **274**, 28059–28062.
13. Hui-Yuen,J., Koganti,S. and Bhaduri-McIntosh,S. (2014) Human B cell immortalization for monoclonal antibody production. *Methods Mol. Biol.*, **1131**, 183–189.
14. Hui-Yuen,J., McAllister,S., Koganti,S., Hill,E. and Bhaduri-McIntosh,S. (2011) Establishment of Epstein–Barr Virus growth-transformed lymphoblastoid cell lines. *J. Vis. Exp.*, e3321, https://doi.org/10.3791/3321.
15. Xu,H., Perez,R.D., Frey,T.R., Burton,E.M., Mannemuddhu,S., Haley,J.D., McIntosh,M.T. and Bhaduri-McIntosh,S. (2019) Novel replisome-associated proteins at cellular replication forks in EBV-transformed B lymphocytes. *PLoS Pathog.*, **15**, e1008228.
16. Paoletti,A.C., Parmely,T.J., Tomomori-Sato,C., Sato,S., Zhu,D., Conaway,R.C., Conaway,J.W., Florens,L. and Washburn,M.P. (2006) Quantitative proteomic analysis of distinct mammalian Mediator complexes using normalized spectral abundance factors. *Proc. Natl. Acad. Sci. U.S.A.*, **103**, 18928–18933.
17. Hulsen,T., de Vlieg,J. and Alkema,W. (2008) BioVenn - a web application for the comparison and visualization of biological lists using area-proportional Venn diagrams. *Bmc Genomics (Electronic Resource)*, **9**, 488.
18. Liao,Y., Wang,J., Jaehnig,E.J., Shi,Z. and Zhang,B. (2019) WebGestalt 2019: gene set analysis toolkit with revamped UIs and APIs. *Nucleic Acids Res.*, **47**, W199–W205.
19. Szklarczyk,D., Gable,A.L., Nastou,K.C., Lyon,D., Kirsch,R., Pyysalo,S., Doncheva,N.T., Legeay,M., Fang,T., Bork,P., *et al.* (2021) The STRING database in 2021: customizable protein-protein networks, and functional characterization of user-uploaded gene/measurement sets. *Nucleic Acids Res.*, **49**, D605–D612.
20. Dembowski,J.A., Dremel,S.E. and DeLuca,N.A. (2017) Replication-coupled recruitment of viral and cellular factors to Herpes simplex virus type 1 replication forks for the maintenance and expression of viral genomes. *PLoS Pathog.*, **13**, e1006166.
21. Li,X., Burton,E.M. and Bhaduri-McIntosh,S. (2017) Chloroquine triggers Epstein–Barr virus replication through phosphorylation

of KAP1/TRIM28 in Burkitt lymphoma cells. *PLoS Pathog.*, **13**, e1006249.
22. Koganti,S., de la Paz,A., Freeman,A.F. and Bhaduri-McIntosh,S. (2014) B lymphocytes from patients with a hypomorphic mutation in STAT3 resist Epstein–Barr virus-driven cell proliferation. *J. Virol.*, **88**, 516–524.
23. Xu,H., Akinyemi,I.A., Chitre,S.A., Loeb,J.C., Lednicky,J.A., McIntosh,M.T. and Bhaduri-McIntosh,S. (2022) SARS-CoV-2 viroporin encoded by ORF3a triggers the NLRP3 inflammatory pathway. *Virology*, **568**, 13–22.
24. Liu,Y., Zheng,Z., Shu,B., Meng,J., Zhang,Y., Zheng,C., Ke,X., Gong,P., Hu,Q. and Wang,H. (2016) SUMO modification stabilizes enterovirus 71 polymerase 3D to facilitate viral replication. *J. Virol.*, **90**, 10472–10485.
25. Li,X., Burton,E.M., Koganti,S., Zhi,J., Doyle,F., Tenenbaum,S.A., Horn,B. and Bhaduri-McIntosh,S. (2018) KRAB-ZFP repressors enforce quiescence of oncogenic Human herpesviruses. *J. Virol.*, **92**, e00298-18.
26. Sheng,Y., Wei,J., Yu,F., Xu,H., Yu,C., Wu,Q., Liu,Y., Li,L., Cui,X.L., Gu,X., *et al.* (2021) A critical role of nuclear m6A reader YTHDC1 in leukemogenesis by regulating MCM complex-mediated DNA replication. *Blood*, **138**, 2838–2852.
27. Schneider,C.A., Rasband,W.S. and Eliceiri,K.W. (2012) NIH image to ImageJ: 25 years of image analysis. *Nat. Methods*, **9**, 671–675.
28. Xu,H., Li,X., Rousseau,B.A., Akinyemi,I.A., Frey,T.R., Zhou,K., Droske,L.E., Mitchell,J.A., McIntosh,M.T. and Bhaduri-McIntosh,S. (2022) IFI16 Partners with KAP1 to maintain Epstein–Barr virus latency. *J. Virol.*, **96**, e0102822.
29. Frey,T.R., Brathwaite,J., Li,X., Burgula,S., Akinyemi,I.A., Agarwal,S., Burton,E.M., Ljungman,M., McIntosh,M.T. and Bhaduri-McIntosh,S. (2020) Nascent transcriptomics reveal cellular prolytic factors upregulated upstream of the latent-to-lytic switch protein of Epstein–Barr Virus. *J. Virol.*, **94**, e01966-19.
30. Cheng,J., Kang,X., Zhang,S. and Yeh,E.T. (2007) SUMO-specific protease 1 is essential for stabilization of HIF1alpha during hypoxia. *Cell*, **131**, 584–595.
31. Bursomanno,S., McGouran,J.F., Kessler,B.M., Hickson,I.D. and Liu,Y. (2015) Regulation of SUMO2 target proteins by the proteasome in human cells exposed to replication stress. *J. Proteome Res.*, **14**, 1687–1699.
32. Adams,A. (1987) Replication of latent Epstein–Barr virus genomes in Raji cells. *J. Virol.*, **61**, 1743–1746.
33. Chiu,Y.F. and Sugden,B. (2016) Epstein–Barr virus: the path from latent to productive infection. *Annu Rev Virol*, **3**, 359–372.
34. Chang,Y.H., Lee,C.P., Su,M.T., Wang,J.T., Chen,J.Y., Lin,S.F., Tsai,C.H., Hsieh,M.J., Takada,K. and Chen,M.R. (2012) Epstein–Barr virus BGLF4 kinase retards cellular S-phase progression and induces chromosomal abnormality. *PLoS One*, **7**, e39217.
35. Flemington,E.K. (2001) Herpesvirus lytic replication and the cell cycle: arresting new developments. *J. Virol.*, **75**, 4475–4481.
36. Rodriguez,A., Armstrong,M., Dwyer,D. and Flemington,E. (1999) Genetic dissection of cell growth arrest functions mediated by the Epstein–Barr virus lytic gene product, Zta. *J. Virol.*, **73**, 9029–9038.
37. Rodriguez,A., Jung,E.J. and Flemington,E.K. (2001) Cell cycle analysis of Epstein–Barr virus-infected cells following treatment with lytic cycle-inducing agents. *J. Virol.*, **75**, 4482–4489.
38. Paladino,P., Marcon,E., Greenblatt,J. and Frappier,L. (2014) Identification of herpesvirus proteins that contribute to G1/S arrest. *J. Virol.*, **88**, 4480–4492.
39. Cayrol,C. and Flemington,E. (1996) G0/G1 growth arrest mediated by a region encompassing the basic leucine zipper (bZIP) domain of the Epstein–Barr virus transactivator Zta. *J. Biol. Chem.*, **271**, 31799–31802.
40. Cayrol,C. and Flemington,E.K. (1996) The Epstein–Barr virus bZIP transcription factor zta causes G0/G1 cell cycle arrest through induction of cyclin-dependent kinase inhibitors. *EMBO J.*, **15**, 2748–2759.
41. Wu,F.Y., Chen,H., Wang,S.E., ApRhys,C.M., Liao,G., Fujimuro,M., Farrell,C.J., Huang,J., Hayward,S.D. and Hayward,G.S. (2003) CCAAT/enhancer binding protein alpha interacts with ZTA and mediates ZTA-induced p21(CIP-1) accumulation and G(1) cell cycle arrest during the Epstein–Barr virus lytic cycle. *J. Virol.*, **77**, 1481–1500.
42. Lilley,C.E., Carson,C.T., Muotri,A.R., Gage,F.H. and Weitzman,M.D. (2005) DNA repair proteins affect the lifecycle of herpes simplex virus 1. *Proc. Natl. Acad. Sci. U.S.A.*, **102**, 5844–5849.
43. Feederle,R., Bannert,H., Lips,H., Muller-Lantzsch,N. and Delecluse,H.J. (2009) The Epstein–Barr virus alkaline exonuclease BGLF5 serves pleiotropic functions in virus replication. *J. Virol.*, **83**, 4952–4962.
44. Wang,J.T., Yang,P.W., Lee,C.P., Han,C.H., Tsai,C.H. and Chen,M.R. (2005) Detection of Epstein–Barr virus BGLF4 protein kinase in virus replication compartments and virus particles. *J. Gen. Virol.*, **86**, 3215–3225.
45. Gershburg,E., Raffa,S., Torrisi,M.R. and Pagano,J.S. (2007) Epstein–Barr virus-encoded protein kinase (BGLF4) is involved in production of infectious virus. *J. Virol.*, **81**, 5407–5412.
46. Morales-Sanchez,A. and Fuentes-Panana,E.M. (2018) The immunomodulatory capacity of an Epstein–Barr Virus abortive lytic cycle: potential contribution to viral tumorigenesis. *Cancers (Basel)*, **10**, 98.
47. Shaban,N.M., Yan,R., Shi,K., Moraes,S.N., Cheng,A.Z., Carpenter,M.A., McLellan,J.S., Yu,Z. and Harris,R.S. (2022) Cryo-EM structure of the EBV ribonucleotide reductase BORF2 and mechanism of APOBEC3B inhibition. *Sci. Adv.*, **8**, eabm2827.
48. Djavadian,R., Chiu,Y.F. and Johannsen,E. (2016) An Epstein–Barr virus-encoded protein complex requires an origin of lytic replication In cis to mediate late gene transcription. *PLoS Pathog.*, **12**, e1005718.
49. Burton,E.M., Akinyemi,I.A., Frey,T.R., Xu,H., Li,X., Su,L.J., Zhi,J., McIntosh,M.T. and Bhaduri-McIntosh,S. (2021) A heterochromatin inducing protein differentially recognizes self versus foreign genomes. *PLoS Pathog.*, **17**, e1009447.
50. King,C.A., Li,X., Barbachano-Guerrero,A. and Bhaduri-McIntosh,S. (2015) STAT3 Regulates lytic activation of Kaposi's sarcoma-associated herpesvirus. *J. Virol.*, **89**, 11347–11355.
51. Li,X., Kozlov,S.V., El-Guindy,A. and Bhaduri-McIntosh,S. (2019) Retrograde regulation by the viral protein kinase epigenetically sustains the Epstein–Barr Virus latency-to-lytic switch to augment virus production. *J. Virol.*, **93**, e00572-19.
52. Orzalli,M.H., Conwell,S.E., Berrios,C., DeCaprio,J.A. and Knipe,D.M. (2013) Nuclear interferon-inducible protein 16 promotes silencing of herpesviral and transfected DNA. *Proc. Natl. Acad. Sci. U.S.A.*, **110**, E4492–E4501.
53. Rauwel,B., Jang,S.M., Cassano,M., Kapopoulou,A., Barde,I. and Trono,D. (2015) Release of human cytomegalovirus from latency by a KAP1/TRIM28 phosphorylation switch. *eLife*, **4**, e06068.
54. Chang,P.C., Fitzgerald,L.D., Van Geelen,A., Izumiya,Y., Ellison,T.J., Wang,D.H., Ann,D.K., Luciw,P.A. and Kung,H.J. (2009) Kruppel-associated box domain-associated protein-1 as a latency regulator for Kaposi's sarcoma-associated herpesvirus and its modulation by the viral protein kinase. *Cancer Res.*, **69**, 5681–5689.
55. Gjyshi,O., Roy,A., Dutta,S., Veettil,M.V., Dutta,D. and Chandran,B. (2015) Activated Nrf2 interacts with Kaposi's Sarcoma-associated herpesvirus latency protein LANA-1 and host protein KAP1 to mediate global lytic gene repression. *J. Virol.*, **89**, 7874–7892.
56. Sun,R., Liang,D., Gao,Y. and Lan,K. (2014) Kaposi's sarcoma-associated herpesvirus-encoded LANA interacts with

host KAP1 to facilitate establishment of viral latency. *J. Virol.*, **88**, 7331–7344.
57. Beauclair,G., Bridier-Nahmias,A., Zagury,J.F., Saib,A. and Zamborlini,A. (2015) JASSA: a comprehensive tool for prediction of SUMOylation sites and SIMs. *Bioinformatics*, **31**, 3483–3491.
58. Zhao,Q., Xie,Y., Zheng,Y., Jiang,S., Liu,W., Mu,W., Liu,Z., Zhao,Y., Xue,Y. and Ren,J. (2014) GPS-SUMO: a tool for the prediction of sumoylation sites and SUMO-interaction motifs. *Nucleic Acids Res.*, **42**, W325–W330.
59. Fredriksson,S., Gullberg,M., Jarvius,J., Olsson,C., Pietras,K., Gustafsdottir,S.M., Ostman,A. and Landegren,U. (2002) Protein detection using proximity-dependent DNA ligation assays. *Nat. Biotechnol.*, **20**, 473–477.
60. Li,M., Xu,X., Chang,C.W. and Liu,Y. (2020) TRIM28 functions as the SUMO E3 ligase for PCNA in prevention of transcription induced DNA breaks. *Proc. Natl. Acad. Sci. U.S.A.*, **117**, 23588–23596.
61. Li,M., Xu,X., Chang,C.W., Zheng,L., Shen,B. and Liu,Y. (2018) SUMO2 conjugation of PCNA facilitates chromatin remodeling to resolve transcription-replication conflicts. *Nat. Commun.*, **9**, 2706.
62. Nguyen,V.T., Giannoni,F., Dubois,M.F., Seo,S.J., Vigneron,M., Kedinger,C. and Bensaude,O. (1996) In vivo degradation of RNA polymerase II largest subunit triggered by alpha-amanitin. *Nucleic Acids Res.*, **24**, 2924–2929.
63. Rudd,M.D. and Luse,D.S. (1996) Amanitin greatly reduces the rate of transcription by RNA polymerase II ternary complexes but fails to inhibit some transcript cleavage modes. *J. Biol. Chem.*, **271**, 21549–21558.
64. Rennekamp,A.J. and Lieberman,P.M. (2010) Initiation of lytic DNA replication in Epstein–Barr virus: search for a common family mechanism. *Future Virol.*, **5**, 65–83.
65. Chiu,Y.F., Sugden,A.U. and Sugden,B. (2013) Epstein–Barr viral productive amplification reprograms nuclear architecture, DNA replication, and histone deposition. *Cell Host Microbe*, **14**, 607–618.
66. Daikoku,T., Kudoh,A., Sugaya,Y., Iwahori,S., Shirata,N., Isomura,H. and Tsurumi,T. (2006) Postreplicative mismatch repair factors are recruited to Epstein–Barr virus replication compartments. *J. Biol. Chem.*, **281**, 11422–11430.
67. Sugimoto,A. (2022) Replication compartments-the great survival strategy for Epstein–Barr Virus lytic replication. *Microorganisms*, **10**, 896.
68. Aygun,O., Xu,X., Liu,Y., Takahashi,H., Kong,S.E., Conaway,R.C., Conaway,J.W. and Svejstrup,J.Q. (2009) Direct inhibition of RNA polymerase II transcription by RECQL5. *J. Biol. Chem.*, **284**, 23197–23203.
69. Izumikawa,K., Yanagida,M., Hayano,T., Tachikawa,H., Komatsu,W., Shimamoto,A., Futami,K., Furuichi,Y., Shinkawa,T., Yamauchi,Y., *et al.* (2008) Association of human DNA helicase RecQ5beta with RNA polymerase II and its possible role in transcription. *Biochem. J.*, **413**, 505–516.
70. Saponaro,M., Kantidakis,T., Mitter,R., Kelly,G.P., Heron,M., Williams,H., Soding,J., Stewart,A. and Svejstrup,J.Q. (2014) RECQL5 controls transcript elongation and suppresses genome instability associated with transcription stress. *Cell*, **157**, 1037–1049.
71. Huang,H., Yu,Z., Zhang,S., Liang,X., Chen,J., Li,C., Ma,J. and Jiao,R. (2010) Drosophila CAF-1 regulates HP1-mediated epigenetic silencing and pericentric heterochromatin stability. *J. Cell Sci.*, **123**, 2853–2861.
72. Smith,S. and Stillman,B. (1989) Purification and characterization of CAF-I, a human cell factor required for chromatin assembly during DNA replication in vitro. *Cell*, **58**, 15–25.
73. Hatanaka,Y., Inoue,K., Oikawa,M., Kamimura,S., Ogonuki,N., Kodama,E.N., Ohkawa,Y., Tsukada,Y. and Ogura,A. (2015) Histone chaperone CAF-1 mediates repressive histone modifications to protect preimplantation mouse embryos from endogenous retrotransposons. *Proc. Natl. Acad. Sci. U.S.A.*, **112**, 14641–14646.
74. Stroud,H., Otero,S., Desvoyes,B., Ramirez-Parra,E., Jacobsen,S.E. and Gutierrez,C. (2012) Genome-wide analysis of histone H3.1 and H3.3 variants in Arabidopsis thaliana. *Proc. Natl. Acad. Sci. U.S.A.*, **109**, 5370–5375.
75. Munz,C. (2019) Latency and lytic replication in Epstein–Barr virus-associated oncogenesis. *Nat. Rev. Micro.*, **17**, 691–700.
76. Chen,C.C. and Mellone,B.G. (2016) Chromatin assembly: journey to the CENter of the chromosome. *J. Cell Biol.*, **214**, 13–24.
77. Hammond,C.M., Stromme,C.B., Huang,H., Patel,D.J. and Groth,A. (2017) Histone chaperone networks shaping chromatin function. *Nat. Rev. Mol. Cell Biol.*, **18**, 141–158.
78. Sauer,P.V., Gu,Y., Liu,W.H., Mattiroli,F., Panne,D., Luger,K. and Churchill,M.E. (2018) Mechanistic insights into histone deposition and nucleosome assembly by the chromatin assembly factor-1. *Nucleic Acids Res.*, **46**, 9907–9917.
79. Rowe,H.M., Jakobsson,J., Mesnard,D., Rougemont,J., Reynard,S., Aktas,T., Maillard,P.V., Layard-Liesching,H., Verp,S., Marquis,J., *et al.* (2010) KAP1 controls endogenous retroviruses in embryonic stem cells. *Nature*, **463**, 237–240.
80. Boehmer,P.E. and Nimonkar,A.V. (2003) Herpes virus replication. *IUBMB Life*, **55**, 13–22.
81. Honess,R.W. and Roizman,B. (1974) Regulation of herpesvirus macromolecular synthesis. I. Cascade regulation of the synthesis of three groups of viral proteins. *J. Virol.*, **14**, 8–19.
82. Kenney,S.C., Arvin,A., Campadelli-Fiume,G., Mocarski,E., Moore,P.S. and Roizman,B. (2007) In: Whitley,R. and Yamanishi,K. (eds.) *Human Herpesviruses: Biology, Therapy, and Immunoprophylaxis*. Cambridge.
83. Tombacz,D., Balazs,Z., Csabai,Z., Moldovan,N., Szucs,A., Sharon,D., Snyder,M. and Boldogkoi,Z. (2017) Characterization of the dynamic transcriptome of a herpesvirus with long-read single molecule real-time sequencing. *Sci. Rep.*, **7**, 43751.
84. Kwiatkowski,D.L., Thompson,H.W. and Bloom,D.C. (2009) The polycomb group protein Bmi1 binds to the herpes simplex virus 1 latent genome and maintains repressive histone marks during latency. *J. Virol.*, **83**, 8173–8181.
85. Wang,Q.Y., Zhou,C., Johnson,K.E., Colgrove,R.C., Coen,D.M. and Knipe,D.M. (2005) Herpesviral latency-associated transcript gene promotes assembly of heterochromatin on viral lytic-gene promoters in latent infection. *Proc. Natl. Acad. Sci. U.S.A.*, **102**, 16055–16059.
86. Reeves,M.B., MacAry,P.A., Lehner,P.J., Sissons,J.G. and Sinclair,J.H. (2005) Latency, chromatin remodeling, and reactivation of human cytomegalovirus in the dendritic cells of healthy carriers. *Proc. Natl. Acad. Sci. U.S.A.*, **102**, 4140–4145.
87. Jang,S.M., Kauzlaric,A., Quivy,J.P., Pontis,J., Rauwel,B., Coluccio,A., Offner,S., Duc,J., Turelli,P., Almouzni,G., *et al.* (2018) KAP1 facilitates reinstatement of heterochromatin after DNA replication. *Nucleic Acids Res.*, **46**, 8788–8802.
88. Cheng,A.Z., Yockteng-Melgar,J., Jarvis,M.C., Malik-Soni,N., Borozan,I., Carpenter,M.A., McCann,J.L., Ebrahimi,D., Shaban,N.M., Marcon,E., *et al.* (2019) Epstein–Barr virus BORF2 inhibits cellular APOBEC3B to preserve viral genome integrity. *Nat. Microbiol.*, **4**, 78–88.
89. Cho,S., Park,J.S. and Kang,Y.K. (2014) AGO2 and SETDB1 cooperate in promoter-targeted transcriptional silencing of the androgen receptor gene. *Nucleic Acids Res.*, **42**, 13545–13556.
90. Bian,C., Chen,Q. and Yu,X. (2015) The zinc finger proteins ZNF644 and WIZ regulate the G9a/GLP complex for gene repression. *eLife*, **4**, e05606.
91. Loyola,A., Tagami,H., Bonaldi,T., Roche,D., Quivy,J.P., Imhof,A., Nakatani,Y., Dent,S.Y. and Almouzni,G. (2009) The HP1alpha-CAF1-SetDB1-containing complex provides H3K9me1 for Suv39-mediated K9me3 in pericentric heterochromatin. *EMBO Rep.*, **10**, 769–775.

92. Liao,G., Huang,J., Fixman,E.D. and Hayward,S.D. (2005) The Epstein–Barr virus replication protein BBLF2/3 provides an origin-tethering function through interaction with the zinc finger DNA binding protein ZBRK1 and the KAP-1 corepressor. *J. Virol.*, **79**, 245–256.
93. Hammarsten,O., Yao,X. and Elias,P. (1996) Inhibition of topoisomerase II by ICRF-193 prevents efficient replication of herpes simplex virus type 1. *J. Virol.*, **70**, 4523–4529.
94. Kawanishi,M. (1993) Topoisomerase I and II activities are required for Epstein–Barr virus replication. *J. Gen. Virol.*, **74**, 2263–2268.
95. Gao,Y. and Pari,G.S. (2009) Interaction of human cytomegalovirus pUL84 with casein kinase 2 is required for oriLyt-dependent DNA replication. *J. Virol.*, **83**, 2393–2396.
96. Yiu,S.P.T., Guo,R., Zerbe,C., Weekes,M.P. and Gewurz,B.E. (2022) Epstein–Barr virus BNRF1 destabilizes SMC5/6 cohesin complexes to evade its restriction of replication compartments. *Cell Rep.*, **38**, 110411.
97. Kudoh,A., Daikoku,T., Ishimi,Y., Kawaguchi,Y., Shirata,N., Iwahori,S., Isomura,H. and Tsurumi,T. (2006) Phosphorylation of MCM4 at sites inactivating DNA helicase activity of the MCM4-MCM6-MCM7 complex during Epstein–Barr virus productive replication. *J. Virol.*, **80**, 10064–10072.
98. Kudoh,A., Iwahori,S., Sato,Y., Nakayama,S., Isomura,H., Murata,T. and Tsurumi,T. (2009) Homologous recombinational repair factors are recruited and loaded onto the viral DNA genome in Epstein–Barr virus replication compartments. *J. Virol.*, **83**, 6641–6651.
99. Sugimoto,A., Kanda,T., Yamashita,Y., Murata,T., Saito,S., Kawashima,D., Isomura,H., Nishiyama,Y. and Tsurumi,T. (2011) Spatiotemporally different DNA repair systems participate in Epstein–Barr virus genome maturation. *J. Virol.*, **85**, 6127–6135.
100. Roseaulin,L.C., Noguchi,C. and Noguchi,E. (2013) Proteasome-dependent degradation of replisome components regulates faithful DNA replication. *Cell Cycle*, **12**, 2564–2569.
101. Ziv,Y., Bielopolski,D., Galanty,Y., Lukas,C., Taya,Y., Schultz,D.C., Lukas,J., Bekker-Jensen,S., Bartek,J. and Shiloh,Y. (2006) Chromatin relaxation in response to DNA double-strand breaks is modulated by a novel ATM- and KAP-1 dependent pathway. *Nat. Cell Biol.*, **8**, 870–876.

Received: July 6, 2023. **Revised:** September 9, 2023. **Editorial Decision:** September 12, 2023. **Accepted:** September 20, 2023